Water Resources Research

RESEARCH ARTICLE
10.1029/2022WR033075

Higher Frozen Soil Permeability Represented in a Hydrological Model Improves Spring Streamflow Prediction From River Basin to Continental Scales

Jetal Agnihotri[1], Ali Behrangi[1,2], Ahmad Tavakoly[3,4], Matthew Geheran[3], Mohammad A. Farmani[1], and Guo-Yue Niu[1]

[1]Department of Hydrology and Atmospheric Sciences, University of Arizona, Tucson, AZ, USA, [2]Department of Geosciences, University of Arizona, Tucson, AZ, USA, [3]Coastal and Hydraulics Laboratory, US Army Engineer Research and Development Center, Vicksburg, MS, USA, [4]Earth System Science Interdisciplinary Center, University of Maryland, College Park, MD, USA

Key Points:

- Streamflow predictions are substantially sensitive to the choice of frozen soil hydraulic property parameterizations
- Irrespective of precipitation product used, a scheme of higher frozen soil permeability yields more skillful streamflow predictions
- Streamflow prediction improvement with a scheme of higher frozen soil permeability is pronounced in basins dominated by frozen ground

Correspondence to:
G.-Y. Niu and A. Behrangi,
niug@email.arizona.edu;
behrangi@arizona.edu

Citation:
Agnihotri, J., Behrangi, A., Tavakoly, A., Geheran, M., Farmani, M. A., & Niu, G.-Y. (2023). Higher frozen soil permeability represented in a hydrological model improves spring streamflow prediction from river basin to continental scales. *Water Resources Research*, *59*, e2022WR033075. https://doi.org/10.1029/2022WR033075

Received 18 JUN 2022
Accepted 14 MAR 2023

Author Contributions:

Conceptualization: Jetal Agnihotri, Ali Behrangi, Ahmad Tavakoly, Guo-Yue Niu
Data curation: Jetal Agnihotri, Mohammad A. Farmani
Formal analysis: Jetal Agnihotri, Ali Behrangi, Ahmad Tavakoly, Mohammad A. Farmani
Funding acquisition: Ali Behrangi, Guo-Yue Niu
Investigation: Jetal Agnihotri, Mohammad A. Farmani, Guo-Yue Niu
Methodology: Jetal Agnihotri, Ali Behrangi, Guo-Yue Niu
Project Administration: Guo-Yue Niu
Software: Ahmad Tavakoly, Matthew Geheran, Mohammad A. Farmani
Supervision: Ali Behrangi, Guo-Yue Niu
Validation: Jetal Agnihotri, Ali Behrangi, Matthew Geheran, Mohammad A. Farmani
Visualization: Jetal Agnihotri, Mohammad A. Farmani

Abstract Despite plentiful evidence of frozen ground effects on snowmelt infiltration from lab experiments at pedon scales, streamflow observations show a weaker or no effect in terms of timing and magnitude at larger scales. We aim to understand this conflicting phenomenon through modeling using the Noah land surface model with multi-physics (MP; Noah-MP) options and the Routing Application for Parallel computatIon of Discharge (RAPID) over the Mississippi River Basin. We conduct 16 experiments with combinations of two supercooled liquid water (SLW) parameterization schemes and four soil hydraulic property schemes in Noah-MP driven by two gridded precipitation products of the North American Land Data Assimilation System (NLDAS) and the Integrated Multi-satellitE Retrievals for GPM (IMERG) Final. We then use RAPID to route Noah-MP modeled surface runoff and groundwater discharge to predict daily streamflow at 52 United States Geological Survey gauges from 2015 to 2019. A model with the highest permeability performs better than other schemes on daily streamflow predictions by 20%–57% throughout a water year and 29%–113% for the spring as measured by the mean Kling-Gupta Efficiency of the 52 gauges. Different SLW schemes demonstrate negligible effects on streamflow predictions. Models forced by IMERG show a better prediction skill compared with those forced by NLDAS at most of the gauges. Both precipitation products confirm that a scheme of higher permeability yields more accurate streamflow predictions over frozen ground. Future models should represent preferential flows through macropore networks to improve the understanding of frozen soil effects on infiltration and discharge across scales.

Plain Language Summary Frozen ground presumably affects the discharge of snowmelt water into rivers during winter and spring due to the apparent effects of ice "blockage." The presence of ice in the soil affects the release of soil liquid water and the time to release the water to local streams and rivers through the effects of soil ice on water flow and capacity to hold snowmelt water. At present, it is not fully understood how the soil ice affects the soil's capability of holding and releasing liquid water to rivers at river-basin to continental scales. We use a computer model to test competing hypotheses through combinations of optional schemes of water holding capacity and water flow. The modeling results over major sub-basins in the Mississippi River show that a model with higher permeable frozen soil results in higher skill in streamflow predictions at river basin scales. This study highlights the need to represent water flow through macropores that may be formed due to ice expansion during freezing/thawing cycles.

1. Introduction

Frozen soil consists of permafrost and seasonally frozen ground (Cuo et al., 2015). Seasonally frozen ground refers to areas where soil is frozen for 15 days or more per year (Y. Zhang et al., 2003), whereas permafrost is defined as the ground that remains below subfreezing temperatures for two or more consecutive years. Permafrost and seasonally frozen ground account for about 58% (or 55 million km^2) of the land surface in the Northern Hemisphere (NSIDC, 2022; T. Zhang et al., 1999), exerting tremendous impacts on water infiltration; ecosystem biogeochemical processes; greenhouse gas emissions; and freshwater, carbon, and nutrient inputs into the Arctic oceans. The presence of ice in soil reduces soil permeability while increasing thermal conductivity, which affects partitioning of snowmelt water into infiltration and surface runoff. At least eight out of the 32 most significant

Writing – original draft: Jetal Agnihotri
Writing – review & editing: Ali Behrangi, Ahmad Tavakoly, Matthew Geheran, Mohammad A. Farmani, Guo-Yue Niu

floods in the 20th century in the United States were related to snowmelt runoff over frozen ground (Berghuijs et al., 2016; Gray et al., 2001; Ivancic & Shaw, 2015; Neri et al., 2019; Perry, 2000; Pradhanang et al., 2013; C. Tang et al., 2012). In addition, snowmelt runoff accounts for three-quarters of annual streamflow in the western US, providing a major water source (Knowles et al., 2006; J. Li et al., 2017). Given the considerable impact of soil freeze-thaw effects on infiltration and runoff, a better understanding of these processes is vital for flood prediction and water resources management as well as for modeling other earth system processes.

At lab scales, the presence of ice in the soil matrix largely reduces soil permeability and substantially modifies water retention characteristics, which represent the relationship between moisture content and suction (Black & Tice, 1989; Gharedaghloo et al., 2020; Kurylyk & Watanabe, 2013; Mohammed et al., 2019; Ren & Vanapalli, 2019). However, many studies have indicated that, at the field scale, the effects of frozen soil on infiltration and runoff are dependent on scale as well as overlying vegetation and snow conditions (Ala-Aho et al., 2021; Bayard et al., 2005; Flanagan et al., 2020; Lindström et al., 2002; Lundberg et al., 2016; Shanley & Chalmers, 1999; Stadler et al., 1996). Shanley and Chalmers (1999) found no clear effects of frozen soil on the runoff ratio in the Sleepers River watershed, Vermont, with an area of 111 km^2. While they did observe a relationship in a 0.59 km^2 agricultural sub-catchment (without vegetation sheltering effects), the data record was insufficient for statistical analysis. The effects of frozen soil on the timing and magnitude of runoff were demonstrated to be very weak from an analysis of 16 years of data from a 0.5 km^2 forested watershed in northern Sweden (Lindström et al., 2002). More field studies using dye tracer techniques (Flury et al., 1994; Stadler et al., 2000; Stähli et al., 2004) revealed that water can infiltrate into deeper soils through preferential pathways depending on pre-freezing water content. The changes in infiltration caused by preferential flow in frozen soil may govern the snowmelt partitioning between surface runoff and infiltration (Larsbo et al., 2019; Lundberg et al., 2016; Mohammed et al., 2021). Air-filled macropore networks allow preferential flow under partially saturated conditions due to substantial increases in infiltration capacity. However, refreezing of infiltrated water can block the preferential pathway (Demand et al., 2019; Larsbo et al., 2019; Mohammed et al., 2019; Stähli et al., 2004; Watanabe & Kugisaki, 2017). The effects of frozen soil on snowmelt infiltration/percolation, surface runoff, groundwater recharge/discharge, and hence streamflow remains "*controversial and contradictory*" and most likely dependent on site, scale, and overlying snow and vegetation conditions as reviewed by Ala-Aho et al. (2021).

Frozen soil models represent soil freeze-thaw processes through coupled heat and flow equations (Richards' equation) as well as the generalized Clapeyron equation for liquid water retention (Flerchinger & Saxton, 1989; Hansson et al., 2004; Koren et al., 1999; Mohammed et al., 2019; Niu & Yang, 2006; Zhao & Gray, 1997). Land surface models (LSMs) for use in weather and climate models started to explicitly represent soil water phase change during 1990s (e.g., Cherkauer & Lettenmaier, 1999; Koren et al., 1999; Pitman et al., 1999) due to its importance to buffering seasonal temperature variations (e.g., Poutou et al., 2004), biogeochemical processes, and greenhouse gas release. Most of the representations are simplified from more complex models (e.g., Flerchinger & Saxton, 1989; Jordan & Beare, 1991; C. Wang & Yang, 2018; Yu et al., 2018; Zhao & Gray, 1997) by neglecting water vapor and its effects on heat and water flows as reviewed by Q. Li et al. (2010). However, these explicit frozen soil schemes degraded runoff simulation in the boreal regions, and thus the effects of soil ice on infiltration and runoff are suggested not being included in LSMs until more data are available (Pitman et al., 1999).

Early models treated the freezing-thawing processes as drying-wetting processes when parameterizing frozen soil hydraulic properties (SHPs), resulting in extremely low permeability and strong matrix suction in the topsoil (and thus upward flow) during freezing (Cox et al., 1999; Flerchinger & Saxton, 1989; Hansson et al., 2004). Lab experiments and plot-scale field experiments support this assumption (Burt & Williams, 1976; Hansson et al., 2004). These models parameterized hydraulic conductivity and matric potential as a function of liquid water content only. Later LSMs and macroscale hydrological models assumed that early spring snowmelt can infiltrate into frozen soil through preferential pathways or lateral overland flows to locally permeable areas (Granger et al., 1984; Jarvis et al., 2016; Mohammed et al., 2021; Niu & Yang, 2006; Stadler et al., 2000; Stähli et al., 1996). For example, Variable Infiltration Capacity (VIC) introduced a scheme based on subgrid spatial distribution of soil temperature to enhance infiltration, thereby improving spring peak flow predictions (Cherkauer et al., 2003). Niu and Yang (2006) developed a scheme of SHP based on the two-domain modeling of Stähli et al. (1996) to enhance infiltration. In a contrasting approach, the NCAR Community Land Model (CLM4.5; and later versions) reduced the permeability by applying an ice impedance factor in hydraulic conductivity. While the use of the impedance factor reduces biases in spring peak flow simulations for two large river basins, it degrades

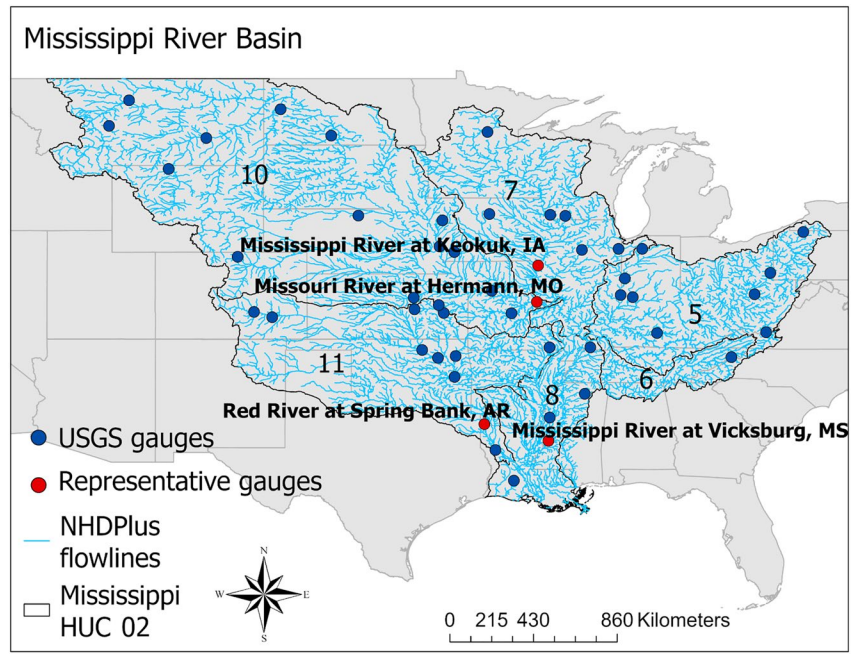

Figure 1. The Mississippi River Basin with 52 United States Geological Survey gauges used in this study. Four gauges (red dots), representing major basins, are selected for further analysis. NHDPlus flowlines are river reaches with Strahler Order higher than three for clarity. The six HUC-2 river basins are the Ohio and Tennessee Rivers (H05 and H06), the Upper Mississippi River (H07), the Lower Mississippi river (H08), the Missouri River (H10), and the Arkansas-White-Red region (H11).

predictions for other watersheds (Swenson et al., 2012). A recent review of field evidence, laboratory studies and physics-based models accounting for freeze-thaw processes (e.g., Larsbo et al., 2019; Mohammed et al., 2021) suggested that macropore flow through preferential pathways (Beven & Germann, 2013; Jarvis et al., 2017) is crucial to predicting infiltration. Despite decades of efforts on lab and field experiments and advanced physically based modeling, there are still knowledge gaps associated with hydrological responses to seasonal frozen ground at basin scales (Ala-Aho et al., 2021).

In this study, we investigate the impacts of soil freeze-thaw parameterizations on streamflow simulations at a large spatial scale and at a high temporal resolution. Specifically, we examine the effects of various frozen soil schemes in the Noah LSM with multi-physics options (Noah-MP) (Niu et al., 2011) on daily simulated discharge at 52 United States Geological Survey (USGS) gauges in the Mississippi River Basin (MRB) using the Routing Application for Parallel omputation of Discharge (RAPID; David et al., 2011) river routing model. Yuan et al. (2018) demonstrate good agreement between streamflow simulations using the Integrated Multi-satellitE Retrievals for GPM (IMERG) Final precipitation and observed data. To address the impacts of uncertainties in climatic forcing on frozen soil effects, we drive Noah-MP with IMERG-Final precipitation and North American Land Data Assimilation System Phase-2 (NLDAS-2) precipitation. While Niu and Yang (2006) tested the impacts of frozen soil SHP schemes on runoff simulations at a monthly resolution without river routing, this study investigates the impact of Noah-MP frozen-soil schemes on streamflow predictions using the RAPID river routing model at a daily scale between 2014 and 2019 for ~1.2 million river reaches over the MRB. This will significantly improve our understanding of the effects of frozen soil at a more application-relevant scale.

2. Materials and Methods

2.1. Study Area

The MRB, covering approximately 41% of the continental United States (CONUS; 3.28 million km^2), comprises six major USGS two-digit hydrologic unit code (HUC-2) (http://water.usgs.gov/GIS/huc.html) basins. These basins, labeled as H05, H06, H07, H08, H10, and H11 (Figure 1), drain to the Ohio, Tennessee, Upper Mississippi, Lower Mississippi, Missouri, and Arkansas-White-Red Rivers, respectively. The regions are delineated by

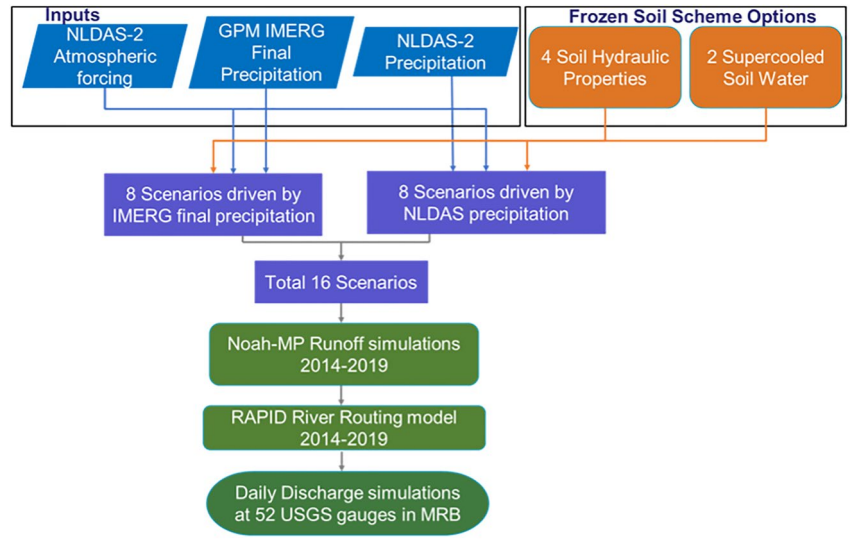

Figure 2. Schematic diagram showing the workflow from the atmospheric forcing data to the RAPID-simulated discharge at gauge stations. Combining the eight frozen soil schemes and the two precipitation products generates 16 model scenarios, from which the resulting modeled surface runoff and groundwater discharge are transferred to RAPID.

the NHDPlus version 2 geospatial data set (Horizon Systems Corporation, 2007), which is an integration of the National Hydrography Data set's (NHD) 1:100,000-scale stream network, 1-arc s National Elevation Data set and the Watershed Boundary Data set. The NHDPlus data set includes approximately 2.7 million vector-based reaches, each of which is associated with a catchment polygon. The NHDPlus version 2 data set, includes NHDPlus catchments, NHDPlus flowlines, and NHDPlus attributes that were used to create a river connectivity file and to calculate flowline slopes. A single data set containing river network and catchment shapefiles for all regions within the MRB (Figure 1) was obtained by merging the flowlines and catchment information from NHDPlus attribute data.

2.2. Description of Data Sets and Models

We used two different precipitation data sets and a data set of other atmospheric forcing variables (see Section 2.2.2) to drive the Noah-MP LSM with optional frozen soil schemes and conducted 16 model experiments. We then transferred surface runoff and groundwater discharge from Noah-MP to RAPID to simulate discharge at the 52 USGS gauge locations in the MRB. Figure 2 shows a schematic diagram for the workflow used in this study, which includes the forcing data, connections between Noah-MP and RAPID river routing model, and modeling outputs. The rest of this section describes in detail forcing and observational data, the Noah-MP LSM, frozen soil schemes, the RAPID river routing model and the model performance evaluation approach used in this study.

2.2.1. Precipitation Forcing Data

We forced Noah-MP with two precipitation data sets: NLDAS-2 precipitation and IMERG-Final Run (V06B) precipitation from 2014 to 2019. The IMERG-Final precipitation data set (Huffman et al., 2020) has been widely applied (Dezfuli et al., 2017; Guo et al., 2016; S. Tang et al., 2020) in modeling studies (Jiang & Bauer-Gottwein, 2019) and shown to often accurately estimate heavy precipitation events (Liu, 2016; Yuan et al., 2018; Zhou et al., 2021). IMERG-Final is a Level-3, half-hourly precipitation data set with a spatial resolution of $0.1° \times 0.1°$ covering 60°S–60°N latitudes. The IMERG algorithm intercalibrates, merges, and interpolates observations from all satellite passive microwave sensors and infrared sensors to produce global precipitation products (Huffman et al., 2020). Regionalization and bias-correction adjustments are applied to the satellite estimates using extensive monthly Global Precipitation Climatology Centre gauge precipitation data to obtain IMERG-Final product. We generated hourly IMERG-Final precipitation by mapping the IMERG half-hourly product from 0.1° to 0.125° (NLDAS-2) resolution using bilinear interpolation.

We also used NLDAS-2 precipitation data (Xia et al., 2012) to drive Noah-MP. This data set features a spatial resolution of 0.125°, an hourly time step, and a period of record from January 1979 to the present over the continental

Table 1
Location and Drainage Area of Four Selected Stations (Red Dots in Figure 1) Used for Further Analysis to Represent Major Basins

Station name	Longitude	Latitude	HUC-2 regions	NHDPlus region	Drainage area (km^2)	
					USGS	NHDPlus
Mississippi River at Keokuk, Iowa	−91.37	40.39	Upper Mississippi Region (H07)	7	308,209	298,719
Missouri River at Hermann, Missouri	−91.44	38.71	Missouri Region (H10)	10	1,353,268	1,277,918
Red River at Spring Bank, Arkansas	−93.86	33.08	Arkansas-White-Red Region (H11)	11	–	146,785
Mississippi River at Vicksburg	−90.91	32.32	Lower Mississipi Region (H08)	8	2,953,881	2,913,317

US (CONUS). The precipitation data is a part of the NLDAS-2 forcing data described in the next section. It is derived from the unified Climate Prediction Centre daily CONUS gauge data set (M. Chen et al., 2008) with Parameter-elevation Regressions on Independent Slopes Model (PRISM; Daly et al., 1994), orographic adjustments, NCEP hourly Stage II doppler radar precipitation data, half-hourly CMORPH (CPC-MORPHing technique (Joyce et al., 2004)) data, and 3-hourly NCEP North American Regional Reanalysis (NARR) data. The precipitation data set benefits from the relative accuracy of the daily gauge product and the temporal and spatial resolution of the Doppler radar and CMORPH data sets.

2.2.2. Other Atmospheric Forcing Data, Vegetation, and Soil Parameters

The IMERG-Final and NLDAS-2 precipitation data sets were each used, along with additional NLDAS-2 atmospheric forcing data, to drive Noah-MP for the 2014–2019 period. The NLDAS-2 data set includes downward shortwave and longwave radiation fluxes, surface air pressure, temperature, specific humidity, and wind speed. These are derived by spatially interpolating and temporally disaggregating the NARR data assimilation product (Mesinger et al., 2006). The NLDAS-2 data set has been widely verified and applied in many modeling studies (Ma et al., 2017; Niu et al., 2020; Pascolini-Campbell et al., 2019; Xia et al., 2012). It is available at an hourly time step with a spatial resolution of 0.125° over the CONUS domain. We used the global 1-km hybrid State Soil Geographic Database and the USGS 24-category vegetation data to determine the soil and vegetation parameters, respectively. Both the 1-km data sets are aggregated to 0.125° with the dominant soil and vegetation types to match the spatial resolution of the NLDAS-2 forcing data. The soil and vegetation parameters are then determined for each soil type and vegetation type through the look-up tables of Noah-MP following Niu et al. (2020).

2.2.3. Observational Data for Model Evaluation

To assess the model's predictive capability, we used the observed daily streamflow data to assess RAPID predicted streamflow time series for the study period (1 January 2015–31 December 2019). The daily streamflow data were downloaded from the US Geological Survey (USGS) National Water Information System (NWIS) website (Accessed at http://nwis.waterdata.usgs.gov/nwis/dvstat/?referred_module=sw). Based on data availability, the observed daily streamflow data at 52 gauges are used in this study for model validation (Figure 1). These gauges represent a wide range of drainage areas, spanning from 178 km^2 (e.g., Bayou De Chien near Clinton, Kentucky) to 2.9 million km^2 (e.g., Mississippi River at Vicksburg). The average discharge recorded at these gauges varies from a low rate of 1.5 m^3/s to a high rate of 23,735 m^3/s. We selected four gauges to represent the major regions for further analysis (red colored dots in Figure 1). The Keokuk, Iowa station represents runoff from the Upper MRB; the Hermann, Missouri station represents the Missouri river basin; the Arkansas-White-Red River basin is represented by the Springbank, Arkansas station; and the Vicksburg, Mississippi station represents the Lower MRB. The drainage area, location, and river basin information for the four selected gauges are summarized in Table 1.

We also used the 4-km gridded snow water equivalent (SWE) and snow depth developed at the University of Arizona (UA) (Broxton et al., 2016; Dawson et al., 2017; Zeng et al., 2018) to validate the Noah-MP simulated. This product was generated by assimilating recorded SWE, snow depth from snow telemetry (SNOTEL), Cooperative Observer Network (COOP) stations, and PRISM daily precipitation and temperature data. In addition, we used the NASA Soil Moisture Active Passive (SMAP) Level-3 data set (O'Neill et al., 2021) to validate the frozen soil days simulated by Noah-MP. SMAP L3 gridded daily estimates of freeze-thaw are available at 36 km spatial resolution on a cylindrical EASE grid and are transformed to a rectangular grid and downscaled to the 0.125° NLDAS-2 grid for comparison.

2.2.4. Noah-MP Model

We selected Noah-MP (Niu et al., 2011; Yang et al., 2011) in this study due to its wide use in the Weather Research and Forecast and the Unified Forecast System for weather and short-term climate predictions and the National Water Model (NWM) for streamflow and water resources predictions. It also provides optional parameterization schemes of various processes, including frozen soil processes, for testing competing hypotheses. Noah-MP describes the energy and water exchanges between the land ecosystem and the atmosphere using one canopy layer, up to three layers (depending on snow depth) for snowpack, four soil layers with a total depth of 2 m, and an unconfined aquifer below the soil column. To represent surface heterogeneity, a "semi-tile" sub-grid scheme is implemented to separately compute net longwave radiation, latent heat, sensible heat, and ground heat fluxes over bare and vegetated soil surfaces. It includes a simple bucket-type groundwater model, of which the storage is controlled by the residual of recharge and discharge rates (Niu et al., 2007). The groundwater recharge is formulated as the Darcy flux driven by capillary and gravity forces, thereby representing exchanges of water between the aquifer and the overlying unsaturated soil column. It was designed for use in global climate models to extend the land "memory" of antecedent weather events and act as a climate "buffer" zone through "negative" recharge during dry seasons and dry years. To facilitate its global use, it does not need detailed geological information of deep aquifers but instead uses global soil type data to control the water flows in the soil and groundwater recharge. Noah-MP adopts a TOPMODEL-based runoff scheme (Niu et al., 2005) to compute surface runoff and groundwater discharge, which are parameterized as an exponential function of water-table depth.

Modeling soil ice content and its effects on infiltration and water flow through frozen soils is strongly affected by snow simulations due to the critical thermal insulating effects of snowpack. The previous versions of Noah-MP usually produced less-than-observed SWE, especially in the western US. For instance, the Noah-MP version in the NWM underpredicts SWE compared to SNOTEL measurements due to model representations and atmospheric inputs (Garousi-Nejad & Tarboton, 2022). Therefore, in this study, we updated Noah-MP with our newly developed snow/rain partitioning scheme based on wet-bulb temperature (Y. H. Wang et al., 2019) and two-stream approximation radiation transfer scheme (W. Wang et al., 2022). Under conditions with <95% in relative humidity (mostly over mountains), the former enhances snowfall and SWE, while the latter generally enhances snowmelt due to the penetration of solar radiation into snowpack and the resulting internal solar heating. As such, we calibrated the holding capacity of liquid water (fraction of snowmelt held by snowpack) to a larger value, 0.08 (from 0.03), and thus more liquid water held during daytime can be refrozen at night, resulting in a better agreement with the UA SWE and snow depth product.

We conducted Noah-MP model simulations on an hourly timestep and with 0.125° resolution starting with spatially constant, relatively wet and warm initial conditions (soil moisture = 0.3 m^3 m^{-3} and soil temperature = 287 K) and ran the model for three loops from 2014 to 2019. The first two loops served as the model spin-up processes, and the surface runoff and groundwater discharge from the third loop were transferred to RAPID for routing. The basic options of all processes other than frozen soil used for the Noah-MP runs are listed in Table 2. We ran all the model scenarios at the spatial resolution of the atmospheric forcing variables, that is, 0.125° and hourly timestep. We used the model parameters included in Niu et al. (2020), of which the model parameters in the dynamic vegetation module were manually calibrated to match the MODIS leaf area index data. In this study, we did not calibrate the parameters associated with frozen soil schemes. We ran the model at an hourly timestep but evaluate the modeled river discharge at a daily scale, because sub-daily runoff prediction skill may more strongly rely on precipitation data accuracy rather than model structures. At present, most global and regional precipitation products generally underestimate extreme events, though it is interesting to study the frozen soil effects at sub-daily scale for modeling flash floods.

Noah-MP describes the coupled heat transfer and water flow in the frozen soil and explicitly predicts liquid water and ice volume by assessing the energy excess or deficit needed to change the soil temperature of a layer to the freezing point (Appendix A in Niu and Yang (2006)). Noah-MP solves the mass-based Richards' equation for water flow through frozen soils with a flux upper boundary condition, that is, the infiltration rate on the surface. The infiltration rate is computed as the residual of water incident on the surface minus surface runoff, which is parameterized as the sum of saturation-excess runoff based on the TOPMODEL concept (Niu et al., 2005) and infiltration-excess runoff over the impermeable fraction of frozen ground (Equation 6 in the following section). Presence of ice modifies SHPs and thus the water flow in the soils and groundwater

Table 2
Noah-MP Options Used in This Study

Process	Options	Schemes
Dynamic vegetation	DVEG = 2	Dynamic vegetation
Canopy stomatal resistance	OPT_CRS = 1	Ball-Berry type
Moisture factor for stomatal resistance	OPT_BTR = 1	Plant water stress
Runoff and groundwater	OPT_RUN = 1	TOPMODEL with groundwater
Surface layer exchange coefficient	OPT_SFC = 1	Monin-Obukhov similarity theory (MOST)
Radiation transfer	OPT_RAD = 1	Modified two-stream
Ground snow surface albedo	OPT_ALB = 3	Two-stream radiation scheme (W. Wang et al., 2022)
Precipitation partitioning	OPT_SNF = 5	Wet bulb temperature (Y. H. Wang et al., 2019)
Lower boundary condition for soil temperature	OPT_TBOT = 2	2-m air temperature climatology at 8 m
Snow/soil temperature time scheme	OPT_STC = 1	Semi-implicit
Surface evaporation resistance	OPT_RSF = 1	Sakaguchi and Zeng (2009)
Root profile	OPT_ROOT = 1	Dynamic root (Niu et al., 2020)
Soil water retention model	OPT_WATRET = 1	van Genuchten (1980)

recharge, which is computed as the water exchanges between the bottom soil and the aquifer following the Darcy's law (see Niu et al. (2007) for more detail). Here, we describe two options of supercooled soil water parameterization schemes, four SHP schemes (two are newly added), and the model scenarios generated from their combinations.

2.2.4.1. SLW Schemes

SLW is the liquid water that coexists with ice over a wide range of subfreezing temperatures and can be derived from various forms of freezing-point depression equations. Noah-MP provides two options to solve the liquid water content. Option 1 (SLW1) uses a general form of freezing point depression equation modified following Niu and Yang (2006):

$$\theta_{\mathrm{liq,max}} = \theta_{\mathrm{sat}} \left\{ \frac{10^3 L_f (T - T_{\mathrm{frz}})}{g T \psi_{\mathrm{sat}}} \right\}^{-1/b} \tag{1}$$

where $\theta_{\mathrm{liq,max}}$ [$\mathrm{m^3\ m^{-3}}$] is the maximum liquid water when the soil temperature is below the freezing point, θ_{sat} [$\mathrm{m^3\ m^{-3}}$] is the porosity, L_f [$\mathrm{J\ kg^{-1}}$] is the latent heat of fusion, T (K) and T_{frz} (K) are the soil temperature and freezing point temperatures respectively, ψ_{sat} (m) is the air-entry matric potential at saturation, b is the Clapp-Hornberger parameter and g ($\mathrm{m\ s^{-2}}$) is the gravitational acceleration. Only the amount of liquid water beyond $\theta_{\mathrm{liq,max}}$ is available for freezing, and the amount of actual liquid water that is frozen is dependent on the freezing rate (Niu & Yang, 2006). Option 2 (SLW2) is a variant of freezing point depression equation with an additional term of $(1 + 8\theta_{\mathrm{ice}})^2$ following (Koren et al., 1999):

$$(1 + 8\theta_{\mathrm{ice}})^2 \psi_{\mathrm{sat}} \left(\frac{\theta_{\mathrm{liq,max}}}{\theta_{\mathrm{sat}}} \right)^{-b} = \frac{10^3 L_f (T - T_{\mathrm{frz}})}{g T} \tag{2}$$

This extra term may produce more liquid water due to enhanced soil surface tension caused by the volume expansion during ice crystal formation. This equation needs to be iteratively solved.

2.2.4.2. SHP Schemes

Noah-MP provides two options for soil hydraulic conductivity and soil hydraulic diffusivity under frozen conditions, and we added two other options in this study. Option 1 (SHP1) separates a model grid cell into two fractional domains: a permeable and an impermeable fraction (Niu & Yang, 2006). Over the impermeable area, the infiltration rate is assumed zero, while over the permeable fraction, the hydraulic conductivity (k) and diffusivity

(D) as well as the matric potential (ψ) are parameterized using total soil moisture ($\theta = \theta_{liq} + \theta_{ice}$, where θ_{liq} (m^3 m^{-3}) and θ_{ice} (m^3 m^{-3}) are the liquid water and ice content, respectively):

$$k = (1 - F_{frz})k_{sat}\left(\frac{\theta}{\theta_{sat}}\right)^{2b+3} \tag{3}$$

$$D = (1 - F_{frz})D_{sat}\left(\frac{\theta}{\theta_{sat}}\right)^{b+2} \tag{4}$$

$$\psi = \psi_{sat}\left(\frac{\theta}{\theta_{sat}}\right)^{-b} \tag{5}$$

where k_{sat} (m s^{-1}) and D_{sat} (m^2 s^{-1}) are saturated hydraulic conductivity and saturated hydraulic diffusivity, respectively, which are based soil texture. F_{frz} is the fractional impermeable area. Matric potential is computed using Equation 5 for all the SHP schemes. Equations 3 and 4 indicate that the permeability is linearly reduced by a factor of F_{frz}. F_{frz} at a soil layer is parameterized as a function of θ_{ice} at the layer:

$$F_{frz} = \left(e^{-\alpha\left(1-\frac{\theta_{ice}}{\theta_{sat}}\right)} - e^{-\alpha}\right)/(1 - e^{-\alpha}) \tag{6}$$

where α is an adjustable, scale-dependent parameter ($a = 3$ in this study following Niu and Yang (2006), not calibrated). Equation 6 is modified from Niu and Yang (2006) to scale F_{frz} to 1.0 when $\theta_{ice}/\theta_{sat} = 1.0$. It produces $F_{frz} < \theta_{ice}/\theta_{sat}$ to account for snowmelt water flowing from impermeable to permeable areas, thus allowing for enhanced infiltration.

Option 2 (SHP2) adopts the scheme proposed by Koren et al. (1999) and used in Noah-V3, which produces less permeable frozen soil. Soil hydraulic conductivity and hydraulic diffusivity under frozen conditions are given by:

$$k = k_{sat}\left(\frac{\theta_{liq}}{\theta_{sat}}\right)^{2b+3} \tag{7}$$

$$D = F_{perm} * D_{sat} * \left(\frac{\theta_{liq}}{\theta_{sat}}\right)^{b+2} + \left(1 - F_{perm}\right) * D_{sat} * \left[\min\left(\theta_{liq}, 0.05\right)/\theta_{sat}\right]^{b+2} \tag{8}$$

where the permeable fraction $F_{perm} = 1/\left(1+(500 * \theta_{ice,max})^3\right)$, and $\theta_{ice,max}$ is the maximum soil ice volume (m^3 m^{-3}) out of all layers.

Option 3 (SHP3) uses the formulation of Flerchinger and Saxton (1989) to parameterize frozen SHPs using liquid water only to estimate the soil water fluxes:

$$k = k_{sat}\left(\frac{\theta_{liq}}{\theta_{sat}}\right)^{2b+3} \tag{9}$$

$$D = D_{sat}\left(\frac{\theta_{liq}}{\theta_{sat}}\right)^{b+2} \tag{10}$$

Option 4 (SHP4) calculates hydraulic properties as a function of the ratio of liquid water content to effective soil porosity, which is defined as the residual soil porosity minus ice volume (Hansson et al., 2004; Zhao & Gray, 1997). In addition, the soil hydraulic conductivity accounts for reduction in infiltration by the ice blocking effects through an impedance factor, E ($E = 6.0$ in this study). This scheme was adopted by many LSMs including CLM4.5 (Swenson et al., 2012).

$$k = 10^{-E\theta_{ice}}k_{sat}\left(\frac{\theta_{liq}}{\theta_{sat} - \theta_{ice}}\right)^{2b+3} \tag{11}$$

$$D = 10^{-E\theta_{ice}}D_{sat}\left(\frac{\theta_{liq}}{\theta_{sat} - \theta_{ice}}\right)^{b+2} \tag{12}$$

Table 3
Summary of Supercooled Liquid Water and Soil Hydraulic Propertie Schemes

Schemes	Models/References	Equations	Underlying assumption
SLW 1	Noah-MP Niu and Yang (2006)	Equation 1	A general form of freezing point depression equation widely accepted by many models
SLW 2	Noah V3 Koren et al. (1999)	Equation 2	A variant of freezing point depression equation, producing more liquid water under subzero temperatures
SHP 1	Noah-MP Niu and Yang (2006)	Equations 3–5	Assumes two fractional areas within a model grid, resulting in enhanced permeability compared to other schemes
SHP 2	Noah V3 Koren et al. (1999)	Equations 7 and 8	Assumes freezing process is a drying process for k but considers two domains for D, resulting in low permeability
SHP 3	Simultaneous Heat And Water Model (SHAW) Flerchinger and Saxton (1989)	Equations 9 and 10	Assumes freezing-thawing process is a drying-wetting process for both k and D, largely reducing permeability
SHP 4	Heat And Water Transport in frozen Soils (HAWTS) Zhao and Gray (1997)	Equations 11 and 12	Assumes reduced porosity and a strong impeding effect due to the impedence fator, largely reducing permeability

Option 1 (SHP1) generally produces higher permeability, than do the other three schemes. The SLW and SHP schemes are summarized in Table 3, and the model scenarios, which use combinations of the SLW and SHP schemes, are listed in Table 4.

2.2.5. RAPID River Routing Model

The Routing Application for Parallel computatIon of Discharge (RAPID, David et al., 2011) uses a matrix version of the Muskingum method to compute discharge in river networks made up of thousands of river reaches. RAPID has an extensive history of development and validation and has been widely used for research and operational applications (David et al., 2013; Sikder et al., 2019; Tavakoly et al., 2017, 2021). It has been operationally implemented recently in the European Center for Medium-Range Weather Forecasting (ECMWF, https://geoglows.ecmwf.int/) streamflow model. Moreover, the National Oceanic and Atmospheric Administration (NOAA) NWM (Maidment, 2017) uses RAPID as an alternative river routing model, and it is also used as a modeling component of the Streamflow Prediction tool (Snow et al., 2016). We use daily mean gridded lateral inflow, that is, surface runoff and groundwater discharge outputs from the last of the three 2014–2019 Noah-MP simulation loops, as the forcing to the RAPID model to predict daily discharge in the river network. The NHDPlus V2 data set is used to develop the geospatial framework for the entire MRB following Tavakoly et al. (2017). The performance of the model scenarios is assessed for the 2015–2019 period with model spin-up performed over 2014, following the convention of previous studies (e.g., Tavakoly et al., 2017, 2021). We used the same parameters for each RAPID simulation to eliminate the complicating effects of parameters on the streamflow results, because the main goal of this study is to compare streamflow routing results from different frozen soil schemes in Noah-MP.

2.3. Model Performance Evaluation

Evaluation of model performance is summarized with the Kling-Gupta Efficiency (KGE; Gupta et al., 2009). Given the mathematical limitations of the Nash-Sutcliffe Efficiency (NSE) (Gupta et al., 2009), the alternative metric KGE is widely used in modeling studies as an efficiency criterion for model performance calibration and validation (Hirpa et al., 2018; Imhoff et al., 2020; Nashwan et al., 2019; Tavakoly et al., 2017, 2021). KGE is based on a decomposition of NSE into correlation, variability bias, and mean bias components and reflects the Euclidean distance from an ideal state in scaled space with respect to these components.

Table 4
Model Scenarios

S1	SLW1 and SHP1	S5	SLW2 and SHP1
S2	SLW1 and SHP2	S6	SLW2 and SHP2
S3	SLW1 and SHP3	S7	SLW2 and SHP3
S4	SLW1 and SHP4	S8	SLW2 and SHP4

$$\mathrm{KGE}_{\mathrm{old}} = 1 - \sqrt{(r-1)^2 + (\alpha-1)^2 + (\beta-1)^2} \tag{13}$$

where r is the correlation between observed and simulated flows, α represents error of flow variability, and β represents biases between observed and simulated flows. KGE spans from $-\infty$ to 1, with 1 representing perfect agreement between observed and simulated values.

When the mean observed flow is predicted at every time step, KGE is nonzero (in contrast to NSE) (Hirpa et al., 2018; Knoben et al., 2019). Knoben et al. (2019) proposed rescaling KGE as follows:

$$\mathrm{KGE}_{si} = \frac{\mathrm{KGE}_{old} + 0.4142}{\sqrt{2}} \tag{14}$$

where *si* represents the *i*th scenario, for instance, the KGE value resulting from S5 is denoted as KGE_{s5}. KGE scores above zero indicate that the model outperforms the long-term mean as a predictor, whereas negative scores indicate the opposite. We calculated KGE values using the daily streamflow simulations from 2015 to 2019. The difference in KGE between two scenarios can be greater than 1.0.

3. Results and Discussion

3.1. Noah-MP Model Validation

We evaluated the modeled daily SWE from Noah-MP against the observation-based UA SWE product from 2015 to 2019 for the six HUC-2 river basins in the MRB (Figure 3). As the frozen soil scheme has very small effects on the snow simulations, here we show only the basin-averaged SWE results from Noah-MP with SLW1 and SHP1 driven by the IMERG precipitation (Figure 3). The modeled SWE reproduces the observed SWE averaged over most river basins with slight overestimations in the Missouri and Arkansas-White-Red Rivers. The model efficiency (NSE) is above 0.76 for all river basins except the Lower Mississippi River, where the model slightly underpredicts the observed SWE. Also, Noah-MP closely reproduces the length of the snow season in terms of the starting and ending dates of the snowy season over most grids. The modeled SWE is generally acceptable (though not perfect) for investigating the effects of different SLW and SHP schemes under frozen conditions on streamflow predictions.

We evaluated the annual number of days when the ice content in the first soil layer (10 cm) of a grid cell is greater than zero from the Noah-MP simulations against the SMAP L3 Freeze Thaw (FT) retrieval product, averaged daily from March 2015 to December 2019 over the MRB (Figure 4). Noah-MP predicted 191 maximum frozen days whereas SMAP L3 FT detected 210 days in the entire MRB. The average number of days predicted by Noah-MP as frozen over MRB is slightly greater than that of SMAP L3. For example, Noah-MP simulates 68 average frozen days, about ∼18 days greater than what is detected by SMAP L3. However, it is important to note that the SMAP FT retrieval is based on radiometer observations at 6:00 a.m. descending and 6:00 p.m. ascending half-orbit passes and does not sample the entire diurnal cycle. Also, the SMAP FT retrieval does not distinguish individual contributions from soil, snow, vegetation, and surface water components within a grid cell, and rather it represents the FT signal of the bulk landscape (Y. Kim et al., 2019). In the northeastern part of MRB, SMAP L3 shows a smaller number of frozen days because of the more vegetation cover (which intercepts solar radiation and remains at an unfrozen state during daytime) in this region. The detection of FT is also degraded over complex terrain, during seasonal FT transitions (Podest et al., 2014), presence of thick snow, surface water, and dense vegetation cover (Kerr et al., 2012; O'Neill et al., 2021; Rowlandson et al., 2018; Wigneron et al., 2017). The correlation between SMAP L3 FT frozen days and Noah-MP simulated frozen days is 0.58. Except the northeastern part of MRB that are covered by dense vegetation, Noah-MP modeled and the SMAP FT derived frozen days show an overall agreement. The SMAP FT is the only frozen soil information currently available at the continental scale for model validation. This rough comparison represents a first attempt that may inspire future studies on how to further benefit from the SMAP observations.

3.2. Model Scenarios Evaluation

This section compares modeled streamflow simulations at 52 USGS gauges in the MRB to the observed discharge from USGS NWIS data set at daily scale. We use KGE to evaluate the performance of different model scenarios. The mean KGE for the eight model scenarios increases from 0.32 to 0.46 when they are driven by IMERG, and S5 performs the best with $\mathrm{KGE}_{S5} = 0.46$ (Figure 5). For the NLDAS scenarios, the mean KGE values range from 0.18 to 0.29, and S5 performs the best with $\mathrm{KGE}_{S5} = 0.29$. The lower mean KGE values resulting from the NLDAS scenarios relative to the IMERG scenarios is due only to the two different precipitation products that were used to drive Noah-MP.

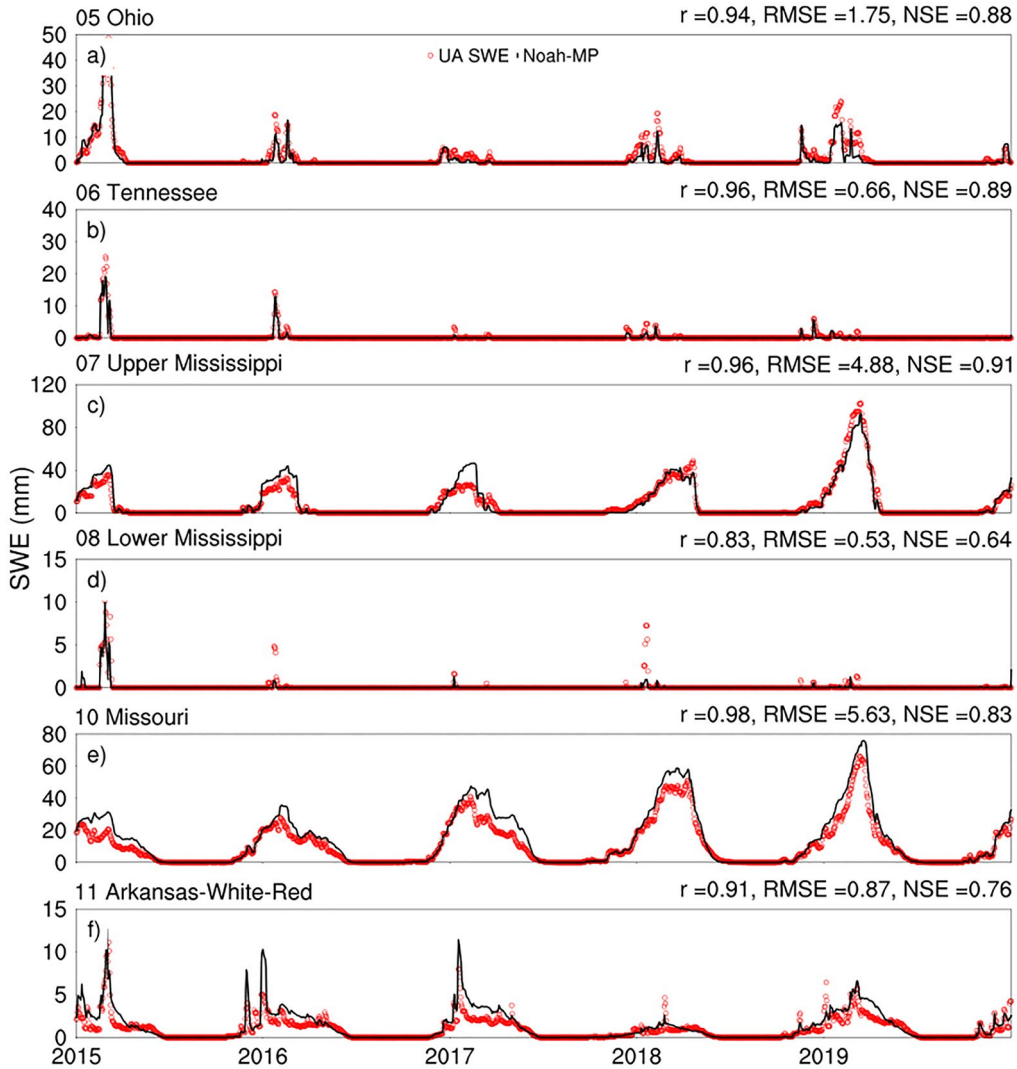

Figure 3. Comparison of the predicted daily snow water equivalent (SWE) (unit mm; black lines) by Noah-MP (S1) and the observation-based University of Arizona SWE product (red dots) from 2015 to 2019 averaged over the HUC-2 basins (Figure 1): (a) the Ohio (H05), (b) Tennessee (H06), (c) Upper Mississippi (H07), (d) Lower Mississippi (H08), (e) Missouri (H10), (f) Arkansas-White-Red (H11). Model evaluation metrics r, RMSE and Nash-Sutcliffe Efficiency are shown on the top of each panel.

We show the model improvement using the percent KGE gain of S5 relative to other scenarios (Figure 6). Positive values indicate a skill gain with S5 relative to the other scenarios, while negative values indicate that a skill loss with S5. S5 performs better at most of the gauges and worse at fewer gauges than do other scenarios (except S1, which shows limited better performance). Model S5 driven by NLDAS precipitation (NLDAS S5) shows a greater KGE gain compared to the other NLDAS scenarios by 5%–12% than that driven by the IMERG precipitation (IMERG S5 compared to other IMERG scenarios) (Table 5). Of all scenarios, regardless of precipitation product used, S7 performs the worst, and S5 and S1, with higher permeability, perform the best. To summarize, implementing SLW1 or SLW2 does not have an apparent effect on model performance, whereas sensitivity to different SHP schemes has a material effect on model performance. The results obtained here are consistent with those by Niu and Yang (2006), where the combination of SHP1 and SLW1 (or SLW2) improve monthly runoff simulations due to consideration of fractional permeable areas with higher permeability.

Model improvement for the months from January to June averaged over years from 2015 to 2019 for daily streamflow simulations is summarized as percent KGE gain (Table 6). We select this period as the snowmelt runoff, infiltration, and groundwater discharge are more strongly affected by the freezing/thawing states of frozen soil,

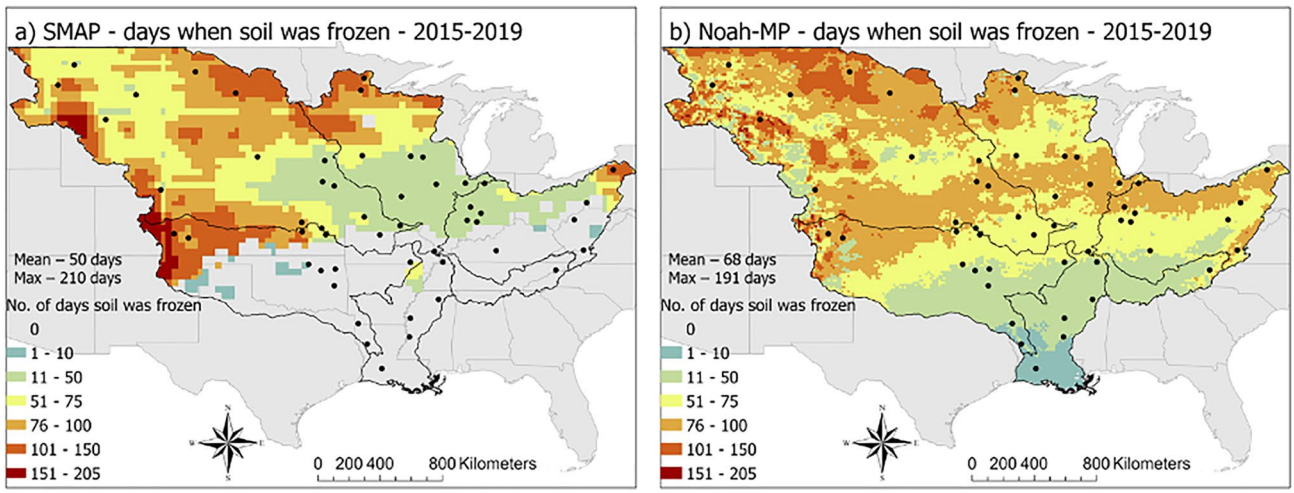

Figure 4. Annual number of days from (a) Soil Moisture Active Passive L3 retrieval of Freeze-Thaw (FT) states and (b) Noah-MP simulations (days when the top 10 cm soil was frozen) averaged for March 2015–December 2019 over the Mississippi River Basin.

further helping the analyses of the model's efficacy to simulate snowmelt-dominated discharge at the gauges. Again, S5 and S1 produce the best model performance, while S7 produces the worst. Differences is model performance are more apparent for the January to June period than for the whole water year. These results support the claim that SHP schemes producing higher permeability yield improved model performance. Consistent with the annual analysis, NLDAS-driven models are more sensitive to the changes in SHP schemes for the seasonal analysis as compared to the IMERG-driven models. IMERG S5 improves the performance over S7 by 64%

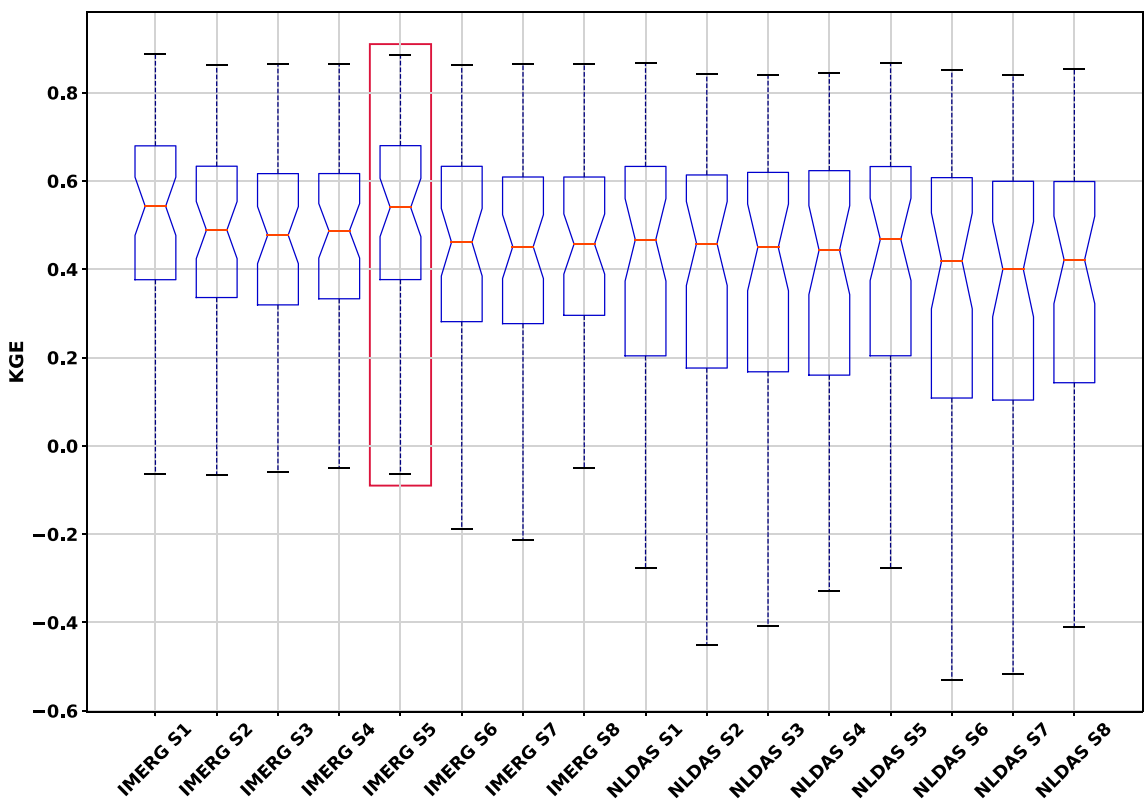

Figure 5. Kling-Gupta efficiency (KGE) resulting from IMERG and NLDAS forced S1 to S8 across the 52 United States Geological Survey gauges in Mississippi River Basin. Boxes are delimited by 25 and 75 percentiles; whiskers show 10th and 90th percentile values, and red line in the box is the median. IMERG S5 performs the best and is selected as the benchmark to measure the percent KGE gain relative to other scenarios.

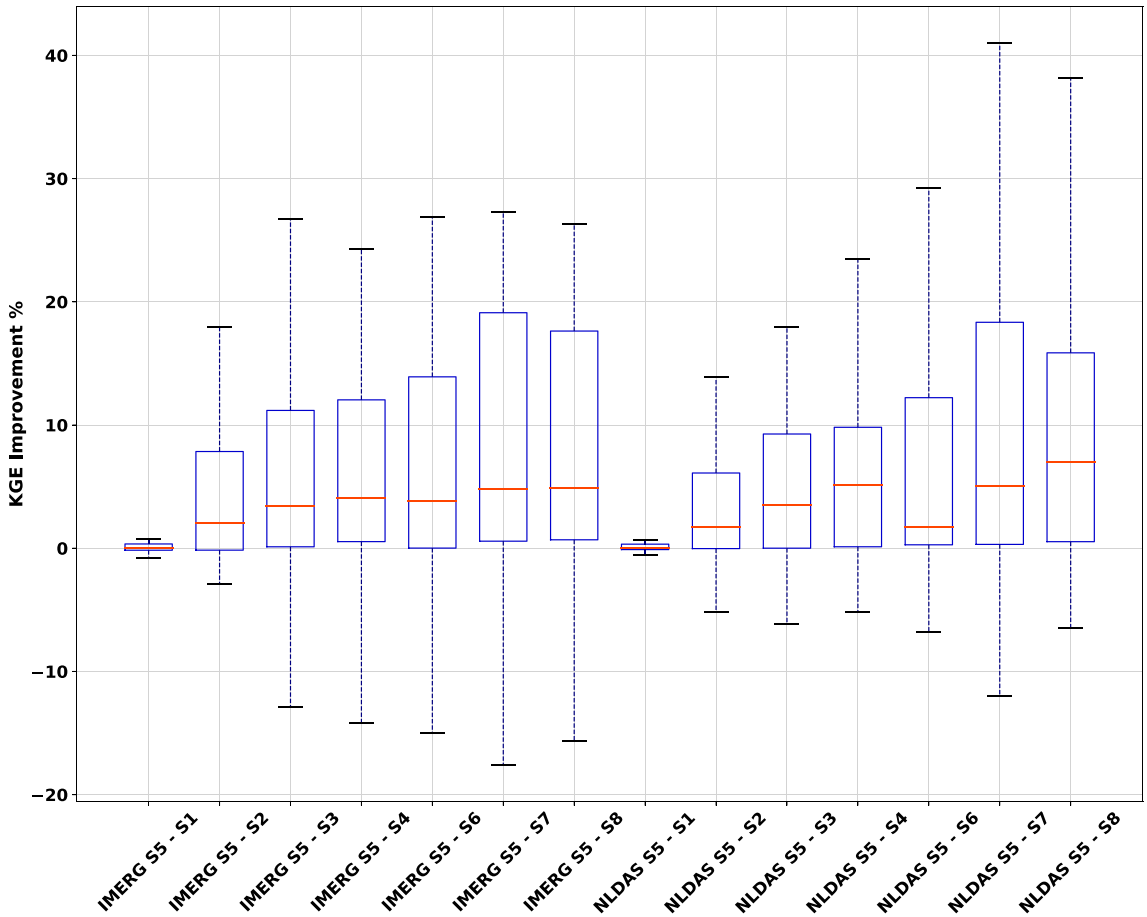

Figure 6. Model improvement (defined by percent KGE gain) of S5 relative to other scenarios driven by IMERG (left panel) and NLDAS (right panel) for all the 52 gauges in the Mississippi River Basin. The boxes are delimited by 25 and 75 percentiles; the whiskers show 10th and 90th percentile values, and the blue line in the box is the median of model improvement. The *Y*-axis is limited to enhance the visibility.

while improvement obtained with NLDAS S5 is 113%. This may suggest that model structure (parameterization schemes) is more critical for model performance when the forcing data (e.g., the NLDAS precipitation) are more uncertain (Figure 6; Table 6).

3.3. Model Scenario Evaluation by Region

The spatial distribution of KGE values from S5 shows satisfactory performance for most gauges for both IMERG-forced (Figure 7a) and NLDAS-forced (Figure 7b) simulations. For instance, about 40 of 52 gauges show KGE values above 0.3 for IMERG S5, while 34 of 52 gauges have KGE values above 0.3 for NLDAS S5. Figure 7c reveals that 32 out of the 52 gauges show improved KGE values for IMERG S5 as compared to NLDAS S5, with a magnitude of improvement of up to 3.1 in KGE. By contrast, the maximum KGE for gauges where NLDAS S5 outperforms IMERG S5 is only 0.46. KGE gain for IMERG S5 relative to NLDAS S5 is greater for the Missouri

Table 5
Mean, Minimum, and Maximum Improvement in KGE (%) Estimated From S5 Compared to Other IMERG and NLDAS Scenarios in Mississippi River Basin for the Whole Water Year From 2015 to 2019

IMERG	S5–S1	S5–S2	S5–S3	S5–S4	S5–S6	S5–S7	S5–S8	Minimum	Maximum
Mean (%)	0	20	26	21	40	45	32	−31	1,243
NLDAS	S5–S1	S5–S2	S5–S3	S5–S4	S5–S6	S5–S7	S5–S8	Minimum	Maximum
Mean (%)	0	25	31	30	49	57	40	−65	2,427

Table 6
Mean, Minimum, and Maximum Improvement in KGE (%) Estimated From S5 Compared to Other IMERG and NLDAS Scenarios in Mississippi River Basin From January to June for 2015–2019

IMERG	S5–S1	S5–S2	S5–S3	S5–S4	S5–S6	S5–S7	S5–S8	Minimum	Maximum
Mean (%)	0	29	39	29	55	64	47	−37	6,441
NLDAS	S5–S1	S5–S2	S5–S3	S5–S4	S5–S6	S5–S7	S5–S8	Minimum	Maximum
Mean (%)	0	49	61	56	94	113	77	−40	958

region (H10) than for the Upper Mississippi Region (H07). Overall, IMERG-forced model simulations produce higher KGE values than those forced by NLDAS, and we mainly consider IMERG scenarios for further analysis.

Figure 8a shows KGE values resulting from IMERG S5, and Figures 8b–8h summarizes the KGE gain by IMERG S5 relative to other IMERG scenarios. IMERG S5 clearly outperforms other IMERG-forced model scenarios at more than 75% of the 52 gauges in the MRB. KGE improvements using IMERG S5 in the Missouri River (H10), which has a greater proportion of soil ice content (see Figure 9), are greater than in all other HUC-2 regions (see Figure 1). This suggests that a higher-permeability frozen soil scheme, such as S5, may promote more accurate simulations of discharge in frozen soil dominated drainage areas. For other HUC-2 regions with less soil ice content (Figure 9), the improvement in KGE is less pronounced.

To further explore the geographic effects, we divide the MRB into East and West regions. The East region consists of the Ohio (H05), Tennessee (H06), Upper Mississippi (H07), and Lower Mississippi (H08) basins of MRB, while the West region consists of the Missouri (H10) and Arkansas-White-Red (H11) basins. Model improvement, as measured by percent KGE gain averaged over the 52 gauges, for IMERG S5 and NLDAS S5 compared to other corresponding scenarios in the East and West regions is presented in Table 7. IMERG S5 shows improvements in the averaged KGE (relative to the worst S7) by up to 203% for the West region but less than 7% in the East region. Also, NLDAS S5 shows improvement in the averaged KGE (relative to the worst, S7 for the east region and S2 for the west) by up to 142% for the West region but less than 8% in the East region. Tavakoly et al. (2017) reported lower KGE values at gauges in the West region from RAPID driven by the VIC (RAPID/VIC) modeled runoff. In this study, IMERG S5 shows a KGE gain at gauges in this region (Tables 7 and 8), suggesting that other models would potentially improve their performance in the West regions, where more soil ice is present (Figure 9), when using a higher-permeability SHP scheme.

3.4. Effects on Hydrograph

This section compares daily discharge simulations with the observed discharges from 2015 to 2019. We used the four gauges representative of the major basins in the MRB (Figure 1) to evaluate the effects of the eight model scenarios on the modeled hydrographs. The gauges representing Ohio and Tennessee regions are not considered due to missing values. These selected gauges represent different HUC-2 regions and reflect a variety of drainage areas (Table 1 and Figure 2) and observed discharges ranging from 1,010 m^3/s to 23,735 m^3/s. IMERG- and NLDAS-driven S5 and S2 are selected for hydrograph analysis since these scenarios include the formulation of SHP following the higher-permeability parameterization of Niu and Yang (2006) and the lower-permeability parameterization of Koren et al. (1999), respectively.

Figure 10 shows the modeled discharge at two gauges: the Missouri River at Hermann, Missouri and the Red River at Spring Bank, Arkansas, which represent the Missouri (H10) and Arkansas-White-Red (H11) regions, respectively. The modeled streamflow at the Spring Bank station agrees well with the observed discharge (KGE >0.84) with both IMERG and NLDAS precipitation products and both scenarios (S5 and S2). Replacing precipitation products or altering SHP and SLW schemes has negligible impacts on the simulated hydrograph at the Spring Bank station (Figure 10a). However, there are substantial differences in the modeled streamflow for the Missouri region. IMERG S5 shows improved performance relative to IMERG S2 with KGE increasing from 0.59 to 0.69 due to the different SHP and SLW schemes. Precipitation has an even greater impact with KGE increasing from 0.53 (NLDAS S5) to 0.69 (IMERG S5). IMERG S5 follows the observed streamflow more closely than the other model scenarios, and IMERG S2 and NLDAS S2 significantly overestimate streamflow and appear to predict peak flow earlier than the gauge data. The dramatic contrasts between scenarios at the

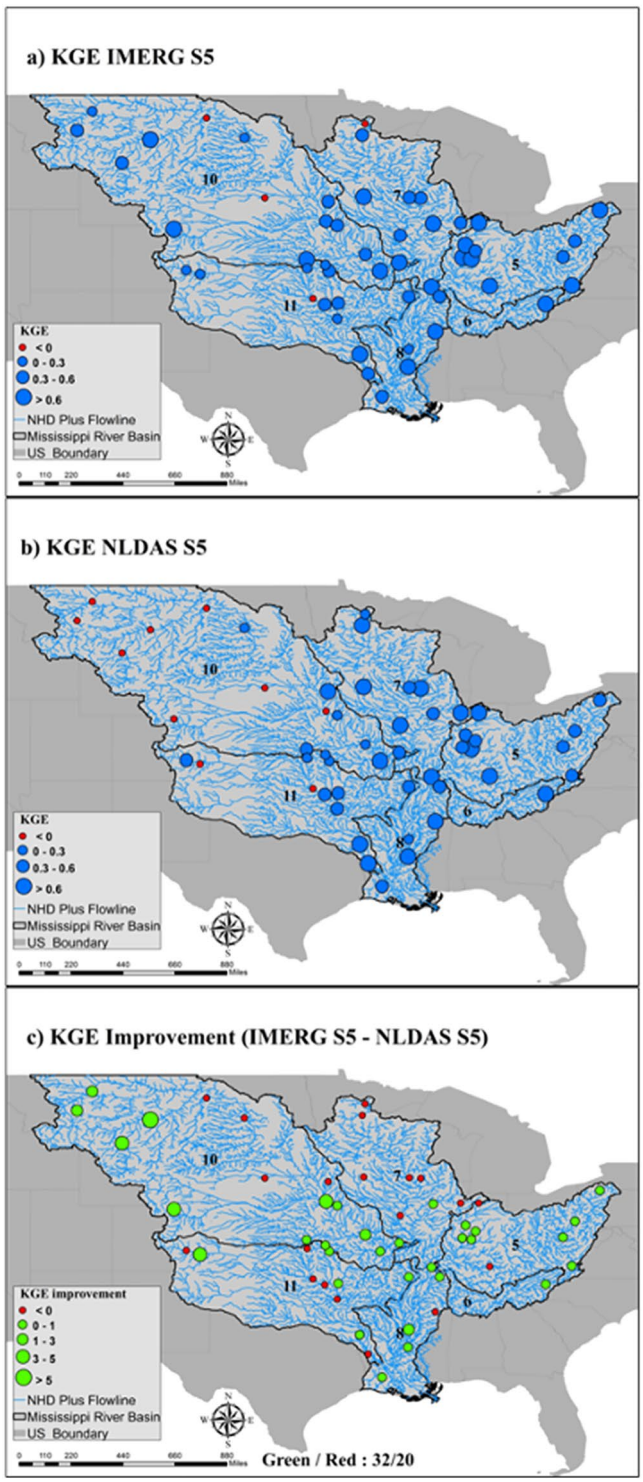

Figure 7. Spatial distribution of KGE at all Mississippi River Basin gauges for (a) IMERG S5, (b) NLDAS S5, and (c) KGE difference between IMERG S5 and NLDAS S5. Red colored dots indicate performance deterioration, while the green colored dots indicate improvement using the IMERG precipitation. The number of Green/Red dots is detailed on ©.

Hermann station suggest that, where the basin is dominated by frozen soil (the Missouri region, H10, Figure 9), the scenario with higher soil permeability (S5) more accurately captures the phase of the hydrograph than the one with lower soil permeability (S2). However, these differences are minor in the Spring Bank station, which is likely due to negligible soil ice present in the basin (Arkansas-White-Red Region, Figure 9).

The model performance is improved for the Vicksburg station (Figure 11a) when IMERG precipitation is used (compared to NLDAS). The scenario differences have minimal impact on the hydrograph at this downstream station with the largest upstream area, which is most likely due to attenuation of the frozen soil effects over the upstream catchments. The hydrograph at the Keokuk station in Iowa demonstrates that NLDAS S5 performs better than other model scenarios, improving KGE from 0.65 (NLDAS S2) to 0.70 (Figure 11). IMERG-forced model scenarios tend to overestimate the streamflow at this station for the years 2016 and 2017, while they are able to capture peak flow more accurately than NLDAS S5 in the year 2019, suggesting potential further improvements through combinations of different precipitation products.

4. Discussion

In this study, we focus on the effects of frozen soil permeability on streamflow predictions at river-basin scales with all the simulations sharing the same soil water retention scheme under freezing conditions, that is, Equation 5. The modeled results suggest a scheme that represents a weaker effect of soil ice on infiltration improves streamflow predictions at most gauges with frozen soil dominated upstream basins. This is also reflected by increases in the modeled ratio of baseflow (or groundwater discharge) to total runoff (Figure 12). IMERG S5 and NLDAS S5, with higher permeability, increase the baseflow ratio by 10.95% and 13.66% compared to IMERG S7 and NLDAS S7, respectively. The increase in baseflow ratio is most pronounced over basins dominated by frozen soil (Figures 12e and 12f). Increases in infiltration during the melting season can propagate into later seasons to increase baseflow ratio through increases in soil moisture and hydraulic conductivity. This study, however, does not investigate the effects of (a) soil water retention characteristics under freezing conditions or (b) preferential flow on streamflow predictions (although it does assume the presence of macropores in the parameterizations given by Equations 3 and 4, which are used in both S1 and S5).

Current understanding of the soil water retention characteristics and SLW content under freezing conditions is still unclear across scales. In a modeling study at pedon scale (Hansson et al., 2004), the soil water retention scheme that treats freezing as drying successfully reproduced the measured evolution of soil water profiles. Due to rapid reduction in soil water potential in the topsoil caused by freezing from the surface, liquid water flows upward across the freezing front. Recent lab experiments suggested even stronger suctions during thawing than during freezing (i.e., hysteresis) due mainly to the supercooled pore water and possibly to changes in pore structure during freezing–thawing processes (Ren & Vanapalli, 2019). These lab-scale experiments and modeling studies suggest that the meltwater is prone to being held rather than draining. This appears to conflict with field experiments on infiltrability of undisturbed soil (Demand et al., 2019; Stadler et al., 1996, 2000) and streamflow observations at catchment scales (Lindström et al., 2002; Shanley

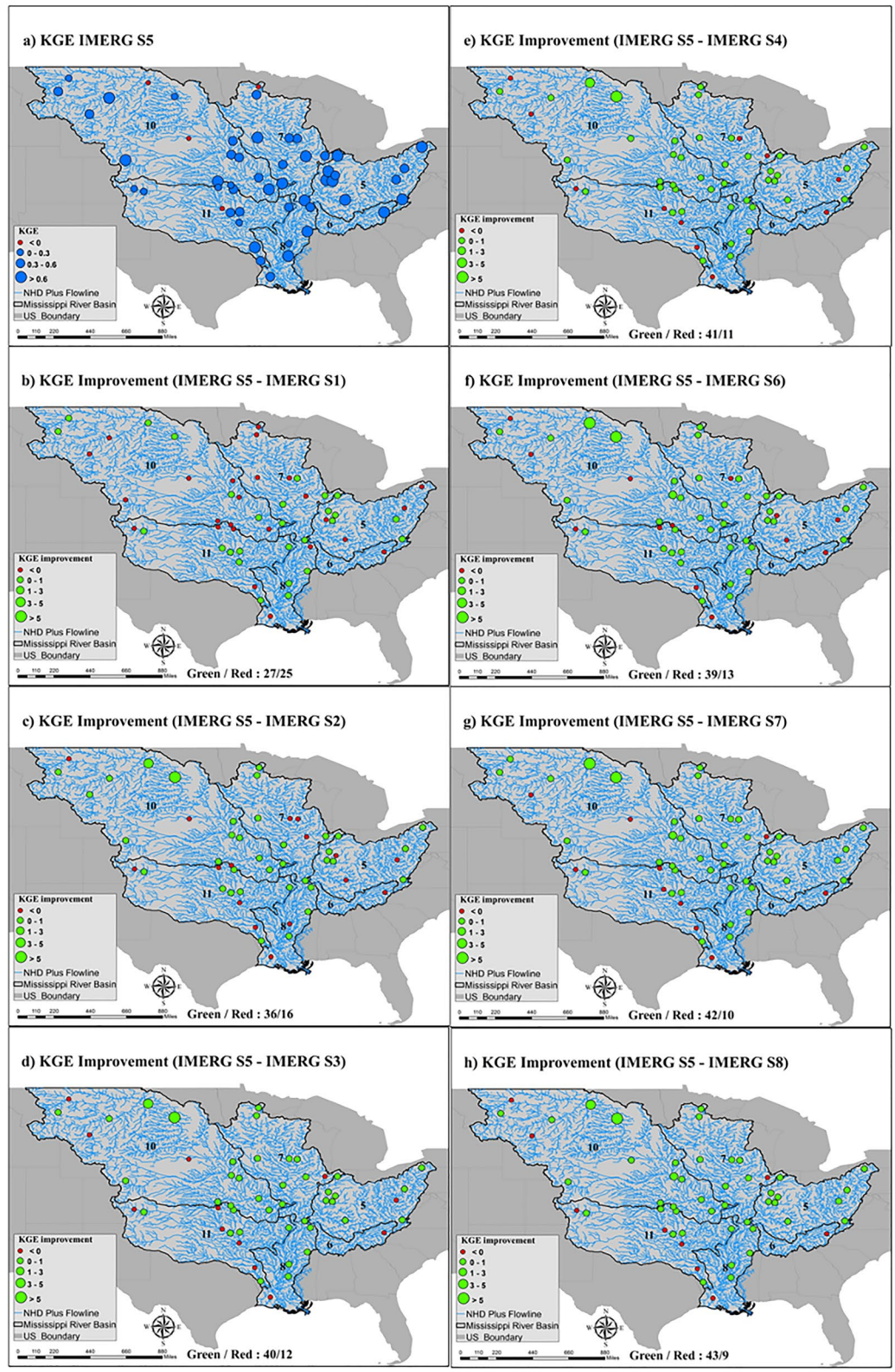

Figure 8. Spatial distribution of IMERG S5 KGE at all Mississippi River Basin gauges (a) and KGE improvement of IMERG S5 over other IMERG scenarios (b–h). Red colored dots indicate performance deterioration, and green colored dots indicate improvement of IMERG S5. The numbers of Green/Red dots are reported on the maps.

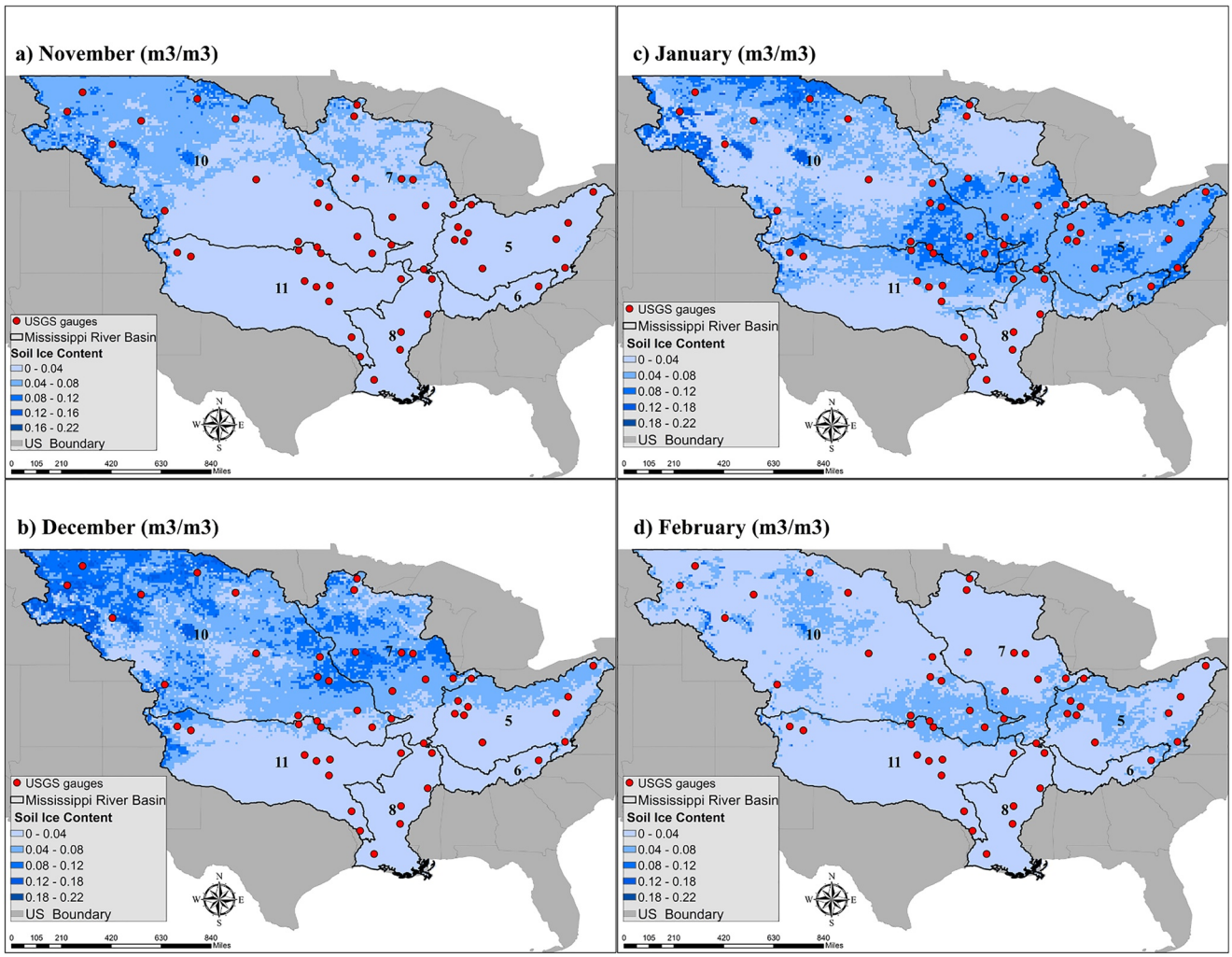

Figure 9. Modeled monthly mean soil ice content (m^3/m^3) in Mississippi River Basin from October to March averaged over 2015–2019. Red dots show United States Geological Survey gauges where streamflow analysis was performed.

Table 7
Differences in KGE (%) Between IMERG S5 and Other IMERG Scenarios Averaged Over Gauges in the West (H10 and H11) and East (H05, H06, H07, and H08) Regions for the Whole Water Year From 2015 to 2019

IMERG							
WEST	S5–S1	S5–S2	S5–S3	S5–S4	S5–S6	S5–S7	S5–S8
Mean (%)	0	58	78	55	178	203	105
EAST	S5–S1	S5–S2	S5–S3	S5–S4	S5–S6	S5–S7	S5–S8
Mean (%)	0	3	5	5	4	7	6
NLDAS							
WEST	S5–S1	S5–S2	S5–S3	S5–S4	S5–S6	S5–S7	S5–S8
Mean (%)	3	142	136	139	121	120	128
EAST	S5–S1	S5–S2	S5–S3	S5–S4	S5–S6	S5–S7	S5–S8
Mean (%)	0	4	6	6	5	8	7

Table 8
Difference in KGE (%) Between IMERG S5 and Other IMERG Scenarios Averaged Over Gauges in the West (H10 and H11) and East (H05, H06, H07, and H08) Regions for Months From January to June of the 2015–2019 Period

IMERG							
WEST	S5–S1	S5–S2	S5–S3	S5–S4	S5–S6	S5–S7	S5–S8
Mean (%)	0	78	109	68	235	280	140
EAST	S5–S1	S5–S2	S5–S3	S5–S4	S5–S6	S5–S7	S5–S8
Mean (%)	0	5	10	9	7	12	11
NLDAS							
WEST	S5–S1	S5–S2	S5–S3	S5–S4	S5–S6	S5–S7	S5–S8
Mean (%)	1	289	248	273	174	171	209
EAST	S5–S1	S5–S2	S5–S3	S5–S4	S5–S6	S5–S7	S5–S8
Mean (%)	0	9	11	11	10	15	14

& Chalmers, 1999) as well as large-scale model studies (Niu & Yang, 2006). The current study suggests that higher permeability of frozen soils with weaker suction of melt water can improve streamflow predictions at basin scales.

The current study does not consider the effects of soil structural change caused by ice expansion during the freezing-thawing cycles, which may alter the pore structure and promote preferential flows through connected macropores. When parameterizing the hydraulic conductivity (Equation 3), a model grid is divided into fractional impermeable and permeable areas, considering presence of macropores following Niu and Yang (2006), but not actually enhancing the K_{sat} values, which are based on soil texture and are around 10^{-6} m/s for most soil types. However, in model simulations considering macropore effects with TOPMODEL-based runoff schemes (J. Chen & Kumar, 2001; Stieglitz et al., 1997), K_{sat} is enhanced by 10^{1}–10^{3} times to account for the presence of macropores in topsoil (Beven & Germann, 1982). In a recent modeling using a more physically based dual-permeability

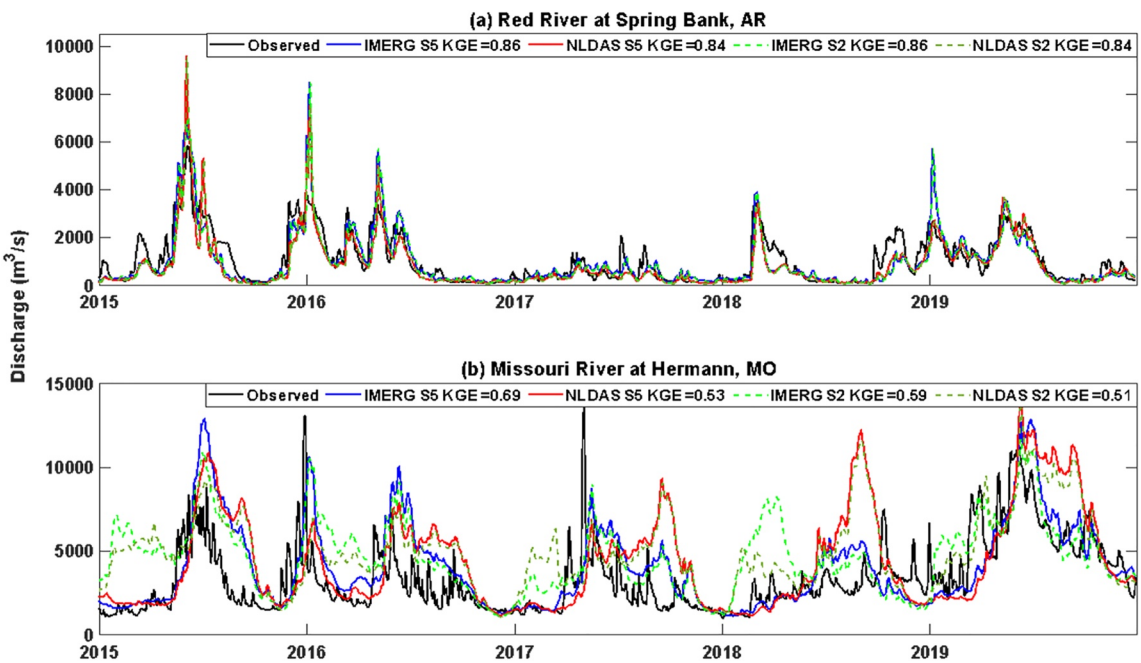

Figure 10. Daily hydrographs of observed and simulated streamflow for (a) the Red River at Spring Bank, Arkansas and (b) the Missouri river at Hermann, Missouri stations, where IMERG and NLDAS S5 and S2 are evaluated over the 2015–2019 period.

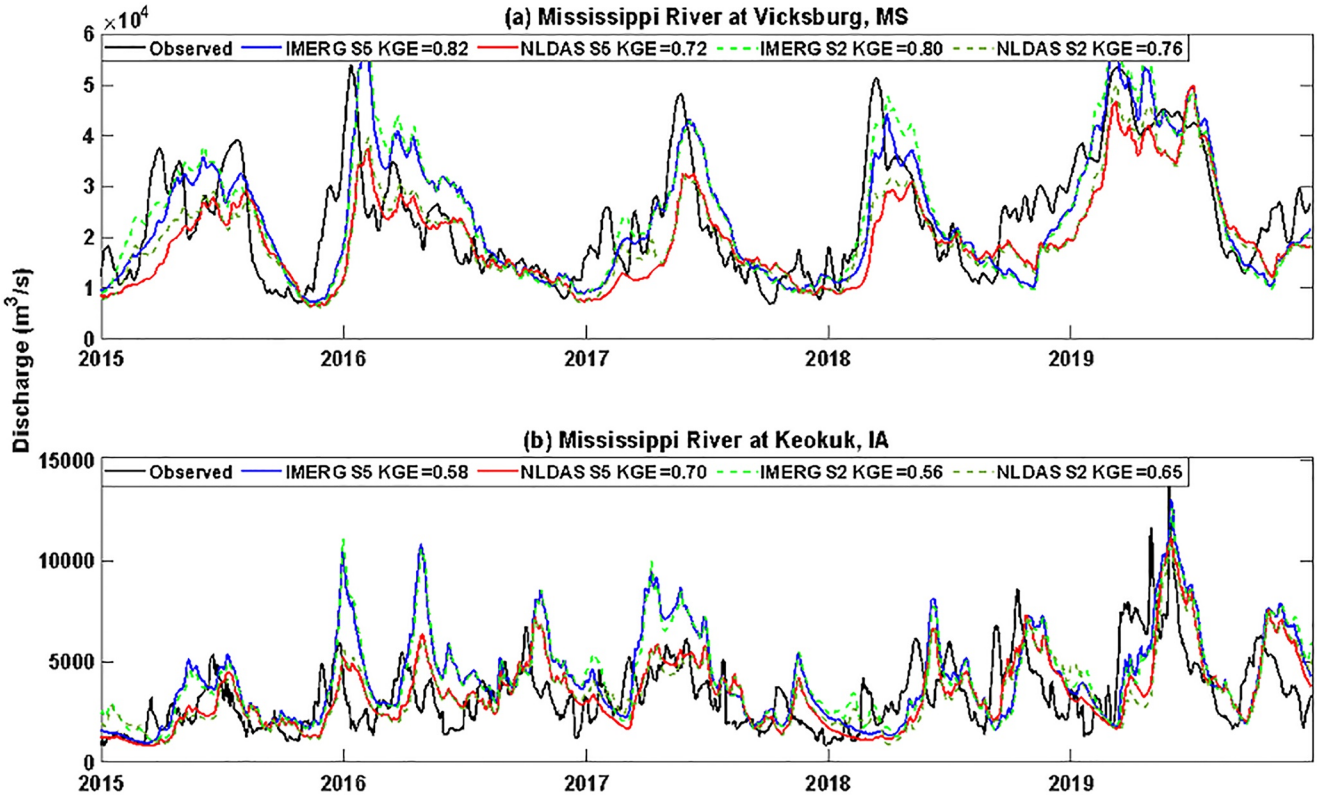

Figure 11. Daily hydrographs of observed and simulated streamflow for (a) the Mississippi River at Vicksburg, Mississippi and (b) the Mississippi River at Keokuk, Iowa, where IMERG and NLDAS S5 and S2 are evaluated over the 2015–2019 period.

model (embedded in HydroGeoSphere), K_{sat} for the macropore domain is calibrated at $\sim 10^{-3}$ m/s to match observed infiltration data under frozen conditions (Mohammed et al., 2021).

Advancements in coupling frozen soil models with 3-dimensional (3D) variably saturated flow models that solve the 3D Richards' equation (J. Chen et al., 2020; Niu et al., 2014; Schilling et al., 2019; Thornton et al., 2022) may help improve the understanding of the impacts of soil freeze-thaw processes on infiltration and flow mechanisms. In these modeling studies, key model parameters (e.g., K_{sat}) were calibrated to improve streamflow simulations, resulting in greater K_{sat} values on the order of 10^{-5} to 10^{-3} m/s. For instance, Niu et al. (2014) calibrated the vertical K_{sat} to 2×10^{-4} m/s and lateral K_{sat} to 2×10^{-3} m/s in the 3D, CATHY/Noah-MP coupled model at 30- and 90-m resolutions in a sub-catchment of the Sleepers River, Vermont. The calibration, however, confused the uncertainties in model structure (or understanding) of key mechanisms controlling flow through porous media (containing soil particles, organic matter, ice, and fractures, etc.) with model parameter uncertainties. To improve the understanding of freeze-thaw processes, model selection techniques should be used to evaluate model structures (or competing hypotheses) while considering model parameter uncertainties (Ye et al., 2008; X. Zhang et al., 2014). Dual permeability flow models that represent slow flow in matrix and rapid flow through macropores both containing ice (e.g., Larsbo et al., 2019; Mohammed et al., 2021) are promising for testing competing hypotheses through alternative model structures (representations of macropore volume fraction, mineral and ice adsorptivity, pore connectivity, and ice blockage, etc.) over a wide range of key parameters with the Bayesian inference criterion (or other objective metrics). In addition, these models provide an opportunity to understand the conflicting phenomena in infiltration and discharge across scales from specific types of soil at lab scales to undisturbed soils at basin scales through the linkage of macropore volume fraction to pre-frozen air-filled pores, ice content, organic matter (Milly et al., 2014), and topographic index (J. Kim & Mohanty, 2017) or through machine-learning aided parameterizations.

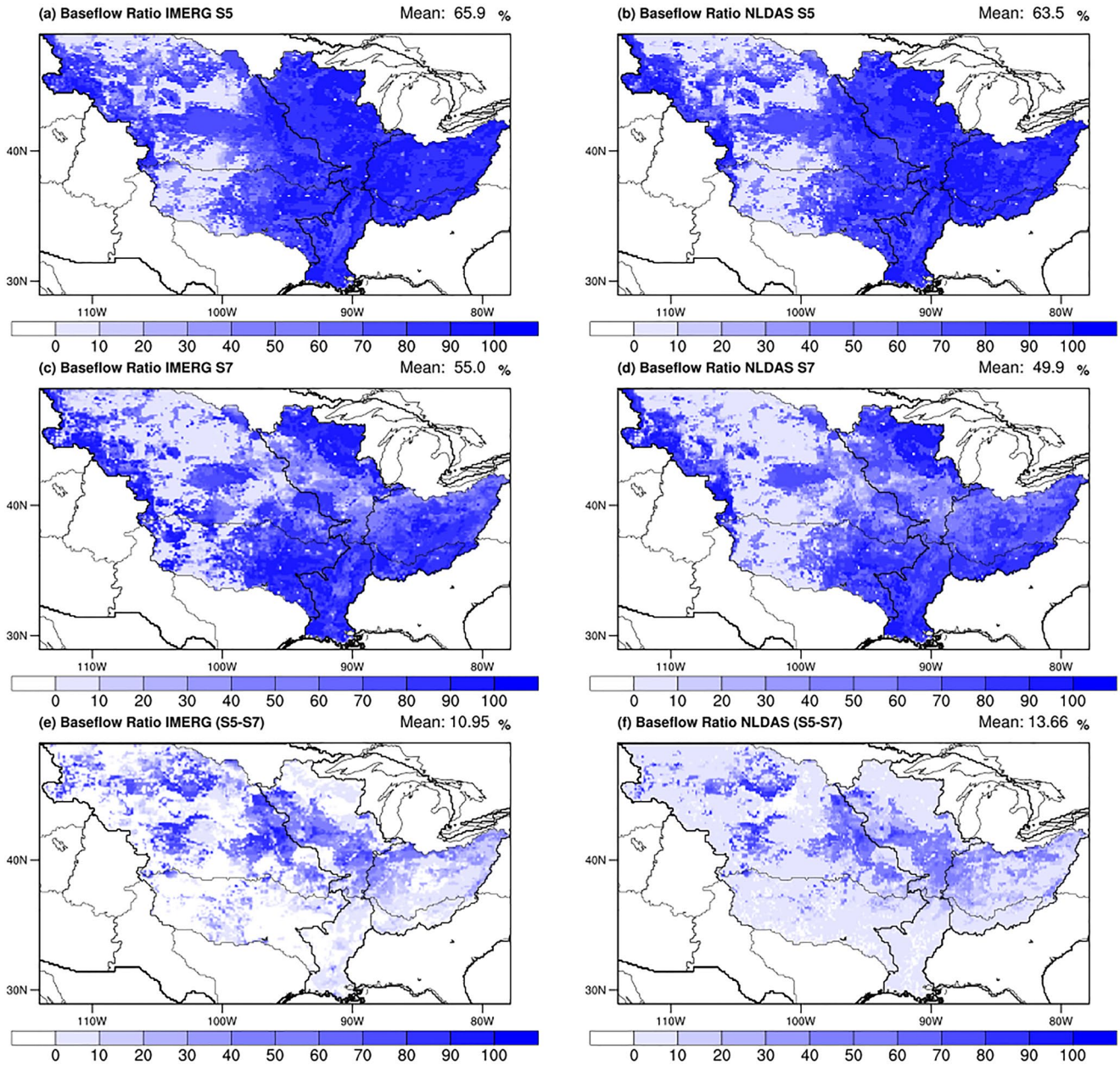

Figure 12. Modeled baseflow ratio of (a) IMERG S5, (b) NLDAS S5, (c) IMERG S7, (d) NLDAS S7, (e) difference between IMERG S5 and IMERG S7, and (f) difference between NLDAS S5 and NLDAS S7 averaged from 2015–2019.

5. Conclusion

In this study, we evaluated the impacts of different representations of frozen soil within the Noah-MP LSM on river discharge simulations. Specifically, we investigated the effects of eight combinations of two SLW schemes and four SHP schemes that featured different hydraulic conductivity parameterizations but the same treatment of matric potential. The gridded hourly surface runoff and groundwater discharge from Noah-MP were transferred to the RAPID river routing model to simulate discharge at 52 USGS gauge locations in the MRB on a daily time step for the 2015–2019 period. We used two hourly precipitation products, NLDAS-2 and GPM IMERG-Final, and other hourly near-surface atmospheric forcing data of NLDAS-2 to drive Noah-MP.

The results demonstrate that parameterization schemes that represent higher permeability in frozen soil produce more accurate streamflow simulations at most gauges in the MRB (39–41 gauges out of 52) relative

to lower-permeability schemes, for example, the SHAW model (Flerchinger & Saxton, 1989; Hansson et al., 2004). While the effects of SLW on streamflow simulations appear to be negligible, simulations appear to be substantially sensitive to SHP schemes. The impacts of frozen soil effects are particularly evident for frozen soil dominated regions. The effects on downstream reaches (with larger upstream drainage areas) appear to be weaker, which may be due to attenuation of the frozen soil effects. Schemes with higher permeability resulted in mean values of KGE improvement over the entire MRB of 20%–57% throughout a water year and 29%–113% for the spring and early summer relative to lower permeability schemes. The number of gauges, where KGE values increased was greater than the number where they decreased. Models forced with IMERG-Final tend to outperform NLDAS driven model scenarios at most of the gauges in the MRB. The results are consistent for the seasonal analysis from January to June when IMERG-driven simulations with increased permeability perform considerably better. In addition, gauges in the western region of the MRB demonstrate considerable improvement in KGE compared to regions in the east, which may be due to the greater amount of soil ice present in the western regions.

This continental-scale study suggests that, irrespective of the precipitation product used to drive the Noah-MP-RAPID model, a model with higher frozen soil permeability (Niu & Yang, 2006) produces more accurate streamflow simulations in frozen-ground dominated drainage areas. The Niu and Yang (2006) model represents a dual domain model with enhanced permeability, but the effects of frozen soil on infiltration and runoff are highly parameterized. Further research investigating the impacts of soil freeze-thaw processes on infiltration and flow mechanisms should rely on physically based models, for example, the dual permeability flow model to represent preferential flow, which should be testable from lab-scale infiltration experiments to basin-scale streamflow simulations.

Data Availability Statement

The data used in this study are freely available online: NLDAS-2 data (http://www.emc.ncep.noaa.gov/mmb/nldas/); the UA SWE and snow depth data (https://nsidc.org/data/nsidc-0719/versions/1); NASA SMAP FT product (https://nsidc.org/data/spl3ftp/versions/3); GPM IMERG-Final product (https://disc.gsfc.nasa.gov/datasets/GPM_3IMERGHH_06/summary); USGS streamflow data (http://nwis.waterdata.usgs.gov/nwis/dvstat/?referred_module=sw). Both the Noah-MP code used in this study and the USGS gauge IDs and data have been uploaded to a repository that may be accessed by other researchers (https://github.com/mfarmani95/Noah_MP).

Acknowledgments
The research carried out for this article was supported by NASA MAP 80NSSC17K0352, NASA PMM Grant 18-PMMST18-0107, and the U.S. Army Corps of Engineers, Engineer Research and Development Center, Coastal Inlets Research Program via Congressionally Directed R&D with the NOAA's National Water Center. Funding for this project was also provided by the NOAA, awarded to the Cooperative Institute for Research on Hydrology through the NOAA Cooperative Agreement with The University of Alabama, NA22NWS4320003. We also thank Aaron Mohammed, Wouter Knoben, and another anonymous reviewer for their constructive comments and suggestions to improve the quality of this paper. The authors would like to dedicate this paper to the first author, Ms. Jetal Agnihotri, who passed away in a recent flood accident. She was a brilliant, passionate, dedicated, and confident young scholar, and we hope to honor her memory with this product of her research.

References

Ala-Aho, P., Autio, A., Bhattacharjee, J., Isokangas, E., Kujala, K., Marttila, H., et al. (2021). What conditions favor the influence of seasonally frozen ground on hydrological partitioning? A systematic review. *Environmental Research Letters*, *16*(4), 043008. https://doi.org/10.1088/1748-9326/abe82c

Bayard, D., Stähli, M., Parriaux, A., & Flühler, H. (2005). The influence of seasonally frozen soil on the snowmelt runoff at two Alpine sites in southern Switzerland. *Journal of Hydrology*, *309*(1–4), 66–84. https://doi.org/10.1016/j.jhydrol.2004.11.012

Berghuijs, W. R., Woods, R. A., Hutton, C. J., & Sivapalan, M. (2016). Dominant flood generating mechanisms across the United States. *Geophysical Research Letters*, *43*(9), 4382–4390. https://doi.org/10.1002/2016gl068070

Beven, K., & Germann, P. (1982). Macropores and water flow in soils. *Water Resources Research*, *18*(5), 1311–1325. https://doi.org/10.1029/WR018i005p01311

Beven, K., & Germann, P. (2013). Macropores and water flow in soils revisited. *Water Resources Research*, *49*(6), 3071–3092. https://doi.org/10.1002/wrcr.20156

Black, P. B., & Tice, A. R. (1989). Comparison of soil freezing curve and soil water curve data for Windsor sandy loam. *Water Resources Research*, *25*(10), 2205–2210. https://doi.org/10.1029/wr025i010p02205

Broxton, P. D., Dawson, N., & Zeng, X. (2016). Linking snowfall and snow accumulation to generate spatial maps of SWE and snow depth. *Earth and Space Science*, *3*(6), 246–256. https://doi.org/10.1002/2016EA000174

Burt, T. P., & Williams, P. J. (1976). Hydraulic conductivity in frozen soils. *Earth Surface Processes*, *1*(4), 349–360. https://doi.org/10.1002/esp.3290010404

Chen, J., & Kumar, P. (2001). Topographic influence on the seasonal and interannual variation of water and energy balance of basins in North America. *Journal of Climate*, *14*(9), 1989–2014. https://doi.org/10.1175/1520-0442(2001)014<1989:tiotsa>2.0.co;2

Chen, J., Sudicky, E. A., Davison, J. H., Frey, S. K., Park, Y. J., Hwang, H. T., et al. (2020). Towards a climate-driven simulation of coupled surface-subsurface hydrology at the continental scale: A Canadian example. *Canadian Water Resources Journal/Revue Canadienne des Ressources Hydriques*, *45*(1), 11–27. https://doi.org/10.1080/07011784.2019.1671235

Chen, M., Shi, W., Xie, P., Silva, V. B. S., Kousky, V. E., Higgins, R. W., & Janowiak, J. E. (2008). Assessing objective techniques for gauge-based analyses of global daily precipitation. *Journal of Geophysical Research*, *113*(4), D04110. https://doi.org/10.1029/2007JD009132

Cherkauer, K. A., Bowling, L. C., & Lettenmaier, D. P. (2003). Variable infiltration capacity cold land process model updates. *Global and Planetary Change*, *38*(1–2), 151–159. https://doi.org/10.1016/S0921-8181(03)00025-0

Cherkauer, K. A., & Lettenmaier, D. P. (1999). Hydrologic effects of frozen soils in the upper Mississippi River basin. *Journal of Geophysical Research*, *104*(D16), 19599–19610. https://doi.org/10.1029/1999JD900337

Cox, P. M., Betts, R. A., Bunton, C. B., Essery, R. L. H., Rowntree, P. R., & Smith, J. (1999). The impact of new land surface physics on the GCM simulation of climate and climate sensitivity. *Climate Dynamics*, *15*(3), 183–203. https://doi.org/10.1007/s003820050276

Cuo, L., Zhang, Y., Bohn, T. J., Zhao, L., Li, J., Liu, Q., & Zhou, B. (2015). Frozen soil degradation and its effects on surface hydrology in the northern Tibetan Plateau. *Journal of Geophysical Research*, *120*(16), 8276–8298. https://doi.org/10.1002/2015JD023193

Daly, C., Neilson, R. P., & Phillips, D. L. (1994). A statistical-topographic model for mapping climatological precipitation over mountainous terrain. *Journal of Applied Meteorology*, *33*(2), 140–158. https://doi.org/10.1175/1520-0450(1994)033<0140:ASTMFM>2.0.CO;2

David, C. H., Maidment, D. R., Niu, G. Y., Yang, Z. L., Habets, F., & Eijkhout, V. (2011). River network routing on the NHDPlus dataset. *Journal of Hydrometeorology*, *12*(5), 913–934. https://doi.org/10.1175/2011JHM1345.1

David, C. H., Yang, Z. L., & Hong, S. (2013). Regional-scale river flow modeling using off-the-shelf runoff products, thousands of mapped rivers and hundreds of stream flow gauges. *Environmental Modelling & Software*, *42*, 116–132. https://doi.org/10.1016/j.envsoft.2012.12.011

Dawson, N., Broxton, P., & Zeng, X. (2017). A new snow density parameterization for land data initialization. *Journal of Hydrometeorology*, *18*(1), 197–207. https://doi.org/10.1175/JHM-D-16-0166.1

Demand, D., Selker, J. S., & Weiler, M. (2019). Influences of macropores on infiltration into seasonally frozen soil. *Vadose Zone Journal*, *18*(1), 1–14. https://doi.org/10.2136/vzj2018.08.0147

Dezfuli, A. K., Ichoku, C. M., Huffman, G. J., Mohr, K. I., Selker, J. S., van de Giesen, N., et al. (2017). Validation of IMERG precipitation in Africa. *Journal of Hydrometeorology*, *18*(10), 2817–2825. https://doi.org/10.1175/JHM-D-17-0139.1

Flanagan, P. X., Mahmood, R., Umphlett, N. A., Haacker, E., Ray, C., Sorensen, W., et al. (2020). A hydrometeorological assessment of the historic 2019 flood of Nebraska, Iowa, and South Dakota. *Bulletin of the American Meteorological Society*, *101*(6), E817–E829. https://doi.org/10.1175/bams-d-19-0101.1

Flerchinger, G. N., & Saxton, K. E. (1989). Simultaneous heat and water model of a freezing snow-residue-soil system. I. Theory and development. *Transactions of the American Society of Agricultural Engineers*, *32*(2), 565–571. https://doi.org/10.13031/2013.31040

Flury, M., Flühler, H., Jury, W. A., & Leuenberger, J. (1994). Susceptibility of soils to preferential flow of water: A field study. *Water Resources Research*, *30*(7), 1945–1954. https://doi.org/10.1029/94wr00871

Garousi-Nejad, I., & Tarboton, D. G. (2022). A comparison of National Water Model retrospective analysis snow outputs at snow telemetry sites across the Western United States. *Hydrological Processes*, *36*(1), e14469.

Gharedaghloo, B., Berg, S. J., & Sudicky, E. A. (2020). Water freezing characteristics in granular soils: Insights from pore-scale simulations. *Advances in Water Resources*, *143*, 103681. https://doi.org/10.1016/j.advwatres.2020.103681

Granger, R. J., Gray, D. M., & Dyck, G. E. (1984). Snowmelt infiltration to frozen Prairie soils. *Canadian Journal of Earth Sciences*, *21*(6), 669–677. https://doi.org/10.1139/e84-073

Gray, D. M., Toth, B., Zhao, L., Pomeroy, J. W., & Granger, R. J. (2001). Estimating areal snowmelt infiltration into frozen soils. *Hydrological Processes*, *15*(16), 3095–3111. https://doi.org/10.1002/hyp.320

Guo, H., Chen, S., Bao, A., Behrangi, A., Hong, Y., Ndayisaba, F., et al. (2016). Early assessment of integrated multi-satellite retrievals for global precipitation measurement over China. *Atmospheric Research*, *176*, 177–133. https://doi.org/10.1016/j.atmosres.2016.02.020

Gupta, H. V., Kling, H., Yilmaz, K. K., & Martinez, G. F. (2009). Decomposition of the mean squared error and NSE performance criteria: Implications for improving hydrological modelling. *Journal of Hydrology*, *377*(1–2), 80–91. https://doi.org/10.1016/j.jhydrol.2009.08.003

Hansson, K., S˘imunek, J., Mizoguchi, M., Lundin, L. C., & Van Genuchten, M. T. (2004). Water flow and heat transport in frozen soil: Numerical solution and freeze–thaw applications. *Vadose Zone Journal*, *3*(2), 693–704. https://doi.org/10.2136/vzj2004.0693

Hirpa, F. A., Salamon, P., Beck, H. E., Lorini, V., Alfieri, L., Zsoter, E., & Dadson, S. J. (2018). Calibration of the Global Flood Awareness System (GloFAS) using daily streamflow data. *Journal of Hydrology*, *566*, 595–606. https://doi.org/10.1016/j.jhydrol.2018.09.052

Horizon Systems Corporation. (2007). National Hydrography Dataset Plus: Documentation. Retrieved from http://www.horizon-systems.com/nhdplus/documentation.php

Huffman, G. J., Bolvin, D. T., Braithwaite, D., Hsu, K., Joyce, R., Kidd, C., et al. (2020). Integrated Multi-satellitE Retrievals for the Global Precipitation Measurement (GPM) mission (IMERG). In V. Levizzani, C. Kidd, D. Kirschbaum, C. Kummerow, K. Nakamura, & F. J. Turk (Eds.), *Chapter 19: Advances in Global Change Research*, *Satellite precipitation measurement* (Vol. 67, pp. 343–353). Springer Nature. https://doi.org/10.1007/978-3-030-24568-9_19

Imhoff, R. O., van Verseveld, W. J., van Osnabrugge, B., & Weerts, A. H. (2020). Scaling point-scale (pedo)transfer functions to seamless large-domain parameter estimates for high-resolution distributed hydrologic modeling: An example for the Rhine River. *Water Resources Research*, *56*(4), e2019WR026807. https://doi.org/10.1029/2019WR026807

Ivancic, T. J., & Shaw, S. B. (2015). Examining why trends in very heavy precipitation should not be mistaken for trends in very high river discharge. *Climatic Change*, *133*(4), 681–693. https://doi.org/10.1007/s10584-015-1476-1

Jarvis, N., Koestel, J., & Larsbo, M. (2016). Understanding preferential flow in the vadose zone: Recent advances and future prospects. *Vadose Zone Journal*, *15*(12), 1–11. https://doi.org/10.2136/vzj2016.09.0075

Jarvis, N., Koestel, J., & Larsbo, M. (2017). Reply to "Comment on 'Understanding preferential low in the vadose zone: Recent advances and future prospects' by N. Jarvis et al.". *Vadose Zone Journal*, *16*(5), 1–4. https://doi.org/10.2136/vzj2017.01.0034r

Jiang, L., & Bauer-Gottwein, P. (2019). How do GPM IMERG precipitation estimates perform as hydrological model forcing? Evaluation for 300 catchments across Mainland China. *Journal of Hydrology*, *572*, 486–500. https://doi.org/10.1016/j.jhydrol.2019.03.042

Jordan, D., & Beare, M. H. (1991). A comparison of methods for estimating soil microbial biomass carbon. *Agriculture, Ecosystems & Environment*, *34*(1–4), 35–41. https://doi.org/10.1016/0167-8809(91)90091-b

Joyce, R. J., Janowiak, J. E., Arkin, P. A., & Xie, P. (2004). CMORPH: A method that produces global precipitation estimates from passive microwave and infrared data at high spatial and temporal resolution. *Journal of Hydrometeorology*, *5*(3), 487–503. https://doi.org/10.1175/1525-7541(2004)005<0487:CAMTPG>2.0.CO;2

Kerr, Y. H., Waldteufel, P., Richaume, P., Wigneron, J. P., Ferrazzoli, P., Mahmoodi, A., et al. (2012). The SMOS soil moisture retrieval algorithm. *IEEE Transactions on Geoscience and Remote Sensing*, *50*(5), 1384–1403. https://doi.org/10.1109/tgrs.2012.2184548

Kim, J., & Mohanty, B. P. (2017). A physically based hydrological connectivity algorithm for describing spatial patterns of soil moisture in the unsaturated zone. *Journal of Geophysical Research: Atmospheres*, *122*(4), 2096–2114. https://doi.org/10.1002/2016jd025591

Kim, Y., Kimball, J. S., Xu, X., Dunbar, R. S., Colliander, A., & Derksen, C. (2019). Global assessment of the SMAP freeze/thaw data record and regional applications for detecting spring onset and frost events. *Remote Sensing*, *11*(11), 1317. https://doi.org/10.3390/rs11111317

Knoben, W. J. M., Freer, J. E., & Woods, R. A. (2019). Technical note: Inherent benchmark or not? Comparing Nash–Sutcliffe and Kling–Gupta efficiency scores. *Hydrology and Earth System Sciences*, *23*(10), 4323–4331. https://doi.org/10.5194/hess-23-4323-2019

Knowles, N., Dettinger, M. D., & Cayan, D. R. (2006). Trends in snowfall versus rainfall in the western United States. *Journal of Climate*, *19*(18), 4545–4559. https://doi.org/10.1175/jcli3850.1

Koren, V., Schaake, J., Mitchell, K., Duan, Q. Y., Chen, F., & Baker, J. M. (1999). A parameterization of snowpack and frozen ground intended for NCEP weather and climate models. *Journal of Geophysical Research*, *104*(D16), 19569–19585. https://doi.org/10.1029/1999jd900232

Kurylyk, B. L., & Watanabe, K. (2013). The mathematical representation of freezing and thawing processes in variably-saturated, non-deformable soils. *Advances in Water Resources*, *60*, 160–177. https://doi.org/10.1016/j.advwatres.2013.07.016

Larsbo, M., Holten, R., Stenrød, M., Eklo, O. M., & Jarvis, N. (2019). A dual-permeability approach for modeling soil water flow and heat transport during freezing and thawing. *Vadose Zone Journal*, *18*(1), 1–11. https://doi.org/10.2136/vzj2019.01.0012

Li, J., Chen, Y., Wang, H., Qin, J., Li, J., & Chiao, S. (2017). Extending flood forecasting lead time in a large watershed by coupling WRF QPF with a distributed hydrological model. *Hydrology and Earth System Sciences*, *21*(2), 1279–1294. https://doi.org/10.5194/hess-21-1279-2017

Li, Q., Sun, S., & Xue, Y. (2010). Analyses and development of a hierarchy of frozen soil models for cold region study. *Journal of Geophysical Research*, *115*(D3), D03107. https://doi.org/10.1029/2009jd012530

Lindström, G., Bishop, K., & Löfvenius, M. O. (2002). Soil frost and runoff at Svartberget, northern Sweden—Measurements and model analysis. *Hydrological Processes*, *16*(17), 3379–3392. https://doi.org/10.1002/hyp.1106

Liu, Z. (2016). Comparison of integrated multisatellite retrievals for GPM (IMERG) and TRMM multisatellite precipitation analysis (TMPA) monthly precipitation products: Initial results. *Journal of Hydrometeorology*, *17*(3), 777–790. https://doi.org/10.1175/JHM-D-15-0068.1

Lundberg, A., Gustafsson, D., Stumpp, C., Kløve, B., & Feiccabrino, J. (2016). Spatiotemporal variations in snow and soil frost—A review of measurement techniques. *Hydrology*, *3*(3), 28. https://doi.org/10.3390/hydrology3030028

Ma, N., Niu, G. Y., Xia, Y., Cai, X., Zhang, Y., Ma, Y., & Fang, Y. (2017). A systematic evaluation of Noah-MP in simulating land-atmosphere energy, water, and carbon exchanges over the continental United States. *Journal of Geophysical Research: Atmospheres*, *122*(22), 12245–12268. https://doi.org/10.1002/2017JD027597

Maidment, D. R. (2017). Conceptual framework for the National Flood Interoperability Experiment. *Journal of the American Water Resources Association*, *53*(2), 245–257. https://doi.org/10.1111/1752-1688.12474

Mesinger, F., DiMego, G., Kalnay, E., Mitchell, K., Shafran, P. C., Ebisuzaki, W., et al. (2006). North American regional reanalysis. *Bulletin of the American Meteorological Society*, *87*(3), 343–360. https://doi.org/10.1175/BAMS-87-3-343

Milly, P. C., Malyshev, S. L., Shevliakova, E., Dunne, K. A., Findell, K. L., Gleeson, T., et al. (2014). An enhanced model of land water and energy for global hydrologic and earth-system studies. *Journal of Hydrometeorology*, *15*(5), 1739–1761. https://doi.org/10.1175/jhm-d-13-0162.1

Mohammed, A. A., Cey, E. E., Hayashi, M., Callaghan, M. V., Park, Y. J., Miller, K. L., & Frey, S. K. (2021). Dual-permeability modeling of preferential flow and snowmelt partitioning in frozen soils. *Vadose Zone Journal*, *20*(2), e20101. https://doi.org/10.1002/vzj2.20101

Mohammed, A. A., Pavlovskii, I., Cey, E. E., & Hayashi, M. (2019). Effects of preferential flow on snowmelt partitioning and groundwater recharge in frozen soils. *Hydrology and Earth System Sciences*, *23*(12), 5017–5031. https://doi.org/10.2136/vzj2018.04.0084

Nashwan, M. S., Shahid, S., & Wang, X. (2019). Assessment of satellite-based precipitation measurement products over the hot desert climate of Egypt. *Remote Sensing*, *11*(5), 555. https://doi.org/10.3390/rs11050555

Neri, A., Villarini, G., Slater, L. J., & Napolitano, F. (2019). On the statistical attribution of the frequency of flood events across the US Midwest. *Advances in Water Resources*, *127*, 225–236. https://doi.org/10.1016/j.advwatres.2019.03.019

Niu, G. Y., Fang, Y. H., Chang, L. L., Jin, J., Yuan, H., & Zeng, X. (2020). Enhancing the Noah-MP ecosystem response to droughts with an explicit representation of plant water storage supplied by dynamic root water uptake. *Journal of Advances in Modeling Earth Systems*, *12*(11), e2020MS002062. https://doi.org/10.1029/2020ms002062

Niu, G. Y., Paniconi, C., Troch, P. A., Scott, R. L., Durcik, M., Zeng, X., et al. (2014). An integrated modelling framework of catchment-scale ecohydrological processes: 1. Model description and tests over an energy-limited watershed. *Ecohydrology*, *7*(2), 427–439. https://doi.org/10.1002/eco.1362

Niu, G. Y., & Yang, Z. L. (2006). Effects of frozen soil on snowmelt runoff and soil water storage at a continental scale. *Journal of Hydrometeorology*, *7*(5), 937–952. https://doi.org/10.1175/JHM538.1

Niu, G. Y., Yang, Z. L., Dickinson, R. E., & Gulden, L. E. (2005). A simple TOPMODEL-based runoff parameterization (SIMTOP) for use in global climate models. *Journal of Geophysical Research*, *110*(21), D21106. https://doi.org/10.1029/2005JD006111

Niu, G. Y., Yang, Z. L., Dickinson, R. E., Gulden, L. E., & Su, H. (2007). Development of a simple groundwater model for use in climate models and evaluation with Gravity Recovery and Climate Experiment data. *Journal of Geophysical Research*, *112*(D7), D07103. https://doi.org/10.1029/2006jd007522

Niu, G. Y., Yang, Z. L., Mitchell, K. E., Chen, F., Ek, M. B., Barlage, M., et al. (2011). The community Noah land surface model with multiparameterization options (Noah-MP): 1. Model description and evaluation with local-scale measurements. *Journal of Geophysical Research*, *116*(12), D12109. https://doi.org/10.1029/2010JD015139

NSIDC. (2022). Quick facts, basic science, and information about snow, ice, and why the cryosphere matters. Retrieved from https://nsidc.org/cryosphere/frozenground/whereis_fg.html

O'Neill, P. E., Chan, S., Njoku, E. G., Jackson, T., Bindlish, R., & Chaubell, J. (2021). *L3 radiometer global daily 36 km EASE-grid soil moisture, version 8*. NASA National Snow and Ice Data Center Distributed Active Archive Center. https://doi.org/10.5067/OMHVSRGFX38O

Pascolini-Campbell, M., Seager, R., Williams, A. P., Cook, B. I., & Pinson, A. O. (2019). Dynamics and variability of the spring dry season in the United States southwest as observed in AmeriFlux and NLDAS-2 data. *Journal of Hydrometeorology*, *20*(6), 1081–1102. https://doi.org/10.1175/JHM-D-18-0154.1

Perry, C. A. (2000). *Significant floods in the United States during the 20th century: USGS measures a century of floods*. US Department of the Interior, US Geological Survey.

Pitman, A. J., Slater, A. G., Desborough, C. E., & Zhao, M. (1999). Uncertainty in the simulation of runoff due to the parameterization of frozen soil moisture using the Global Soil Wetness Project methodology. *Journal of Geophysical Research*, *104*(D14), 16879–16888. https://doi.org/10.1029/1999jd900261

Podest, E., McDonald, K. C., & Kimball, J. S. (2014). Multisensor microwave sensitivity to freeze/thaw dynamics across a complex boreal landscape. *IEEE Transactions on Geoscience and Remote Sensing*, *52*(11), 6818–6828. https://doi.org/10.1109/tgrs.2014.2303635

Poutou, E., Krinner, G., Genthon, C., & de Noblet-Ducoudre, N. (2004). Role of soil freezing in future boreal climate change. *Climate Dynamics*, *23*(6), 621–639. https://doi.org/10.1007/s00382-004-0459-0

Pradhanang, S. M., Frei, A., Zion, M., Schneiderman, E. M., Steenhuis, T. S., & Pierson, D. (2013). Rain-on-snow runoff events in New York. *Hydrological Processes*, *27*(21), 3035–3049. https://doi.org/10.1002/hyp.9864

Ren, J., & Vanapalli, S. K. (2019). Comparison of soil-freezing and soil-water characteristic curves of two Canadian soils. *Vadose Zone Journal*, *18*(1), 1–14. https://doi.org/10.2136/vzj2018.10.0185

Rowlandson, T. L., Berg, A. A., Roy, A., Kim, E., Lara, R. P., Powers, J., et al. (2018). Capturing agricultural soil freeze/thaw state through remote sensing and ground observations: A soil freeze/thaw validation campaign. *Remote Sensing of Environment*, *211*, 59–70. https://doi.org/10.1016/j.rse.2018.04.003

Sakaguchi, K., & Zeng, X. (2009). Effects of soil wetness, plant litter, and under-canopy atmospheric stability on ground evaporation in the Community Land Model (CLM3. 5). *Journal of Geophysical Research*, *114*(D1), D01107. https://doi.org/10.1029/2008jd010834

Schilling, O. S., Park, Y. J., Therrien, R., & Nagare, R. M. (2019). Integrated surface and subsurface hydrological modeling with snowmelt and pore water freeze-thaw. *Groundwater*, *57*(1), 63–74. https://doi.org/10.1111/gwat.12841

Shanley, J. B., & Chalmers, A. (1999). The effect of frozen soil on snowmelt runoff at Sleepers River, Vermont. *Hydrological Processes*, *13*(12–13), 1843–1857. https://doi.org/10.1002/(sici)1099-1085(199909)13:12/13<1843::aid-hyp879>3.0.co;2-g

Sikder, M. S., David, C. H., Allen, G. H., Qiao, X., Nelson, E. J., & Matin, M. A. (2019). Evaluation of available global runoff datasets through a river model in support of transboundary water management in South and Southeast Asia. *Frontiers in Environmental Science*, *7*, 171. https://doi.org/10.3389/fenvs.2019.00171

Snow, A. D., Christensen, S. D., Swain, N. R., Nelson, E. J., Ames, D. P., Jones, N. L., et al. (2016). A high-resolution National-Scale Hydrologic Forecast system from a global ensemble land surface model. *Journal of the American Water Resources Association*, *52*(4), 950–964. https://doi.org/10.1111/1752-1688.12434

Stadler, D., Sta¨hli, M., Aeby, P., & Flu¨hler, H. (2000). Dye tracing and image analysis for quantifying water infiltration into frozen soils. *Soil Science Society of America Journal*, *64*(2), 505–516. https://doi.org/10.2136/sssaj2000.642505x

Stadler, D., Wunderli, H., Auckenthaler, A., Flühler, H., & Bründl, M. (1996). Measurement of frost-induced snowmelt runoff in a forest soil. *Hydrological Processes*, *10*(10), 1293–1304. https://doi.org/10.1002/(sici)1099-1085(199610)10:10<1293::aid-hyp461>3.0.co;2-i

Stähli, M., Bayard, D., Wydler, H., & Flühler, H. (2004). Snowmelt infiltration into alpine soils visualized by dye tracer technique. *Arctic Antarctic and Alpine Research*, *36*(1), 128–135. https://doi.org/10.1657/1523-0430(2004)036[0128:SIIASV]2.0.CO;2

Stähli, M., Jansson, P. E., & Lundin, L. C. (1996). Preferential water flow in a frozen soil – A two-domain model approach. *Hydrological Processes*, *10*(10), 1305–1316. https://doi.org/10.1002/(SICI)1099-1085(199610)10:10<1305::AID-HYP462>3.0.CO;2-F

Stieglitz, M., Rind, D., Famiglietti, J., & Rosenzweig, C. (1997). An efficient approach to modeling the topographic control of surface hydrology for regional and global climate modeling. *Journal of Climate*, *10*(1), 118–137. https://doi.org/10.1175/1520-0442(1997)010<0118:aeatmt>2.0.co;2

Swenson, S. C., Lawrence, D. M., & Lee, H. (2012). Improved simulation of the terrestrial hydrological cycle in permafrost regions by the Community Land Model. *Journal of Advances in Modeling Earth Systems*, *4*(8), M08002. https://doi.org/10.1029/2012MS000165

Tang, C., Crosby, B. T., Wheaton, J. M., & Piechota, T. C. (2012). Assessing streamflow sensitivity to temperature increases in the Salmon River Basin, Idaho. *Global and Planetary Change*, *88*, 32–44. https://doi.org/10.1016/j.gloplacha.2012.03.002

Tang, S., Li, R., He, J., Wang, H., Fan, X., & Yao, S. (2020). Comparative evaluation of the GPM IMERG early, late, and final hourly precipitation products using the CMPA data over Sichuan Basin of China. *Water (Switzerland)*, *12*(2), 554. https://doi.org/10.3390/w12020554

Tavakoly, A. A., Gutenson, J. L., Lewis, J. W., Follum, M. L., Rajib, A., LaHatte, W. C., & Hamilton, C. O. (2021). Direct integration of numerous dams and reservoirs outflow in continental scale hydrologic modeling. *Water Resources Research*, *57*(9), e2020WR029544. https://doi.org/10.1029/2020WR029544

Tavakoly, A. A., Snow, A. D., David, C. H., Follum, M. L., Maidment, D. R., & Yang, Z. L. (2017). Continental-scale river flow modeling of the Mississippi River Basin using high-resolution NHDPlus dataset. *Journal of the American Water Resources Association*, *53*(2), 258–279. https://doi.org/10.1111/1752-1688.12456

Thornton, J. M., Therrien, R., Mariéthoz, G., Linde, N., & Brunner, P. (2022). Simulating fully-integrated hydrological dynamics in complex Alpine headwaters: Potential and challenges. *Water Resources Research*, *58*(4), e2020WR029390. https://doi.org/10.1029/2020wr029390

van Genuchten, M. T. (1980). A closed-form equation for predicting the hydraulic conductivity of unsaturated soils1. *Soil Science Society of America Journal*, *44*(5), 892–898.

Wang, C., & Yang, K. (2018). A new scheme for considering soil water-heat transport coupling based on Community Land Model: Model description and preliminary validation. *Journal of Advances in Modeling Earth Systems*, *10*(4), 927–950. https://doi.org/10.1002/2017MS001148

Wang, W., He, C., Moore, J., Wang, G., & Niu, G. Y. (2022). Physics-based narrowband optical parameters for snow albedo simulation in climate models. *Journal of Advances in Modeling Earth Systems*, *14*(1), e2020MS002431. https://doi.org/10.1029/2020ms002431

Wang, Y. H., Broxton, P., Fang, Y., Behrangi, A., Barlage, M., Zeng, X., & Niu, G. Y. (2019). A wet-bulb temperature-based rain-snow partitioning scheme improves snowpack prediction over the drier western United States. *Geophysical Research Letters*, *46*(23), 13825–13835. https://doi.org/10.1029/2019gl085722

Watanabe, K., & Kugisaki, Y. (2017). Effect of macropores on soil freezing and thawing with infiltration. *Hydrological Processes*, *31*(2), 270–278. https://doi.org/10.1002/hyp.10939

Wigneron, J. P., Jackson, T. J., O'neill, P., De Lannoy, G., de Rosnay, P., Walker, J. P., et al. (2017). Modelling the passive microwave signature from land surfaces: A review of recent results and application to the L-band SMOS & SMAP soil moisture retrieval algorithms. *Remote Sensing of Environment*, *192*, 238–262. https://doi.org/10.1016/j.rse.2017.01.024

Xia, Y., Mitchell, K., Ek, M., Sheffield, J., Cosgrove, B., Wood, E., et al. (2012). Continental-scale water and energy flux analysis and validation for the North American land data assimilation system project phase 2 (NLDAS-2): 1. Intercomparison and application of model products. *Journal of Geophysical Research*, *117*(3). https://doi.org/10.1029/2011JD016048

Yang, Z. L., Niu, G. Y., Mitchell, K. E., Chen, F., Ek, M. B., Barlage, M., et al. (2011). The community Noah land surface model with multiparameterization options (Noah-MP): 2. Evaluation over global river basins. *Journal of Geophysical Research*, *116*(D12), D12110. https://doi.org/10.1029/2010jd015140

Ye, M., Meyer, P. D., & Neuman, S. P. (2008). On model selection criteria in multimodel analysis. *Water Resources Research*, *44*(3), W03428. https://doi.org/10.1029/2008wr006803

Yu, L., Zeng, Y., Wen, J., & Su, Z. (2018). Liquid-vapor-air flow in the frozen soil. *Journal of Geophysical Research: Atmospheres*, *123*, 7393–7415. https://doi.org/10.1029/2018JD028502

Yuan, F., Wang, B., Shi, C., Cui, W., Zhao, C., Liu, Y., et al. (2018). Evaluation of hydrological utility of IMERG-Final run V05 and TMPA 3B42V7 satellite precipitation products in the Yellow River source region, China. *Journal of Hydrology*, *567*, 696–711. https://doi.org/10.1016/j.jhydrol.2018.06.045

Zeng, X., Broxton, P., & Dawson, N. (2018). Snowpack change from 1982 to 2016 over conterminous United States. *Geophysical Research Letters*, *45*(23), 12940–12947. https://doi.org/10.1029/2018GL079621

Zhang, T., Barry, R. G., Knowles, K., Heginbottom, J. A., & Brown, J. (1999). Statistics and characteristics of permafrost and ground-ice distribution in the Northern Hemisphere. *Polar Geography*, *23*(2), 132–154. https://doi.org/10.1080/10889379909377670

Zhang, X., Niu, G. Y., Elshall, A. S., Ye, M., Barron-Gafford, G. A., & Pavao-Zuckerman, M. (2014). Assessing five evolving microbial enzyme models against field measurements from a semiarid savannah—What are the mechanisms of soil respiration pulses? *Geophysical Research Letters*, *41*(18), 6428–6434. https://doi.org/10.1002/2014gl061399

Zhang, Y., Ohata, T., & Kadota, T. (2003). Land-surface hydrological processes in the permafrost region of the eastern Tibetan Plateau. *Journal of Hydrology*, *283*(1–4), 41–56. https://doi.org/10.1016/S0022-1694(03)00240-3

Zhao, L., & Gray, D. M. (1997). A parametric expression for estimating infiltration into frozen soils. *Hydrological Processes*, *11*(13), 1761–1775. https://doi.org/10.1002/(sici)1099-1085(19971030)11:13<1761::aid-hyp604>3.0.co;2-o

Zhou, C., Gao, W., Hu, J., Du, L., & Du, L. (2021). Capability of IMERG V6 early, late, and final precipitation products for monitoring extreme precipitation events. *Remote Sensing*, *13*(4), 689. https://doi.org/10.3390/rs13040689